

IN THIS ISSUE

Two Ways to Measure Temperature Feature Simplicity, Accuracy, and Flexibility

Thermocouples are widely used for measuring temperature. This article suggests two signal conditioning solutions. The first combines reference-junction compensation and signal conditioning in a single analog IC for convenience and ease of use; the second separates the reference-junction compensation from the signal conditioning to provide greater flexibility and accuracy in a digital solution. Page 3.

Inertial Sensors Facilitate Autonomous Operation in Mobile Robots

Ground-based robot systems must often handle dull, dirty, and dangerous tasks in missions where direct human involvement is expensive, dangerous, or ineffective. Some robotic platforms can operate autonomously, using navigation systems to monitor and control their motion. Accuracy is key for useful autonomous operation. MEMS gyroscopes provide a mechanism for optimizing navigation performance. Page 9.

Multichannel DDS Enables Phase-Coherent FSK Modulation

Common single-channel direct-digital synthesizers produce phase-continuous frequency transitions. In Doppler radar, NMR/MRI spectrometry, and other applications, however, phase-coherent transitions are preferred. This article demonstrates how to configure the AD9958/AD9959 multichannel DDS as a robust phase-coherent frequency-shift keyed (FSK) modulator by summing the DDS outputs. Page 13.

High-Side Current Sensing with Wide Dynamic Range: Three Solutions

Precision current sensing allows designers to measure motor torque, dc-to-dc converter efficiency, bias current in a power transistor, and other critical parameters in the presence of high common-mode voltages. This article describes three solutions—discrete, integrated, and application-optimized—that provide high-accuracy, high-resolution current sensing for a variety of applications. Page 15.

Boost Supply and High-Voltage DAC Provide Tuning Signal for Antennas and Filters

Antenna arrays and filters are often tuned by varying the voltage on a barium strontium titanate (BST) capacitor. Voltages applied to this ferroelectric material cause small variations in the crystal structure, changing the dielectric constant and, thus, the capacitance. The capacitor is tuned by applying a voltage of up to 30 V. This article shows an easy way to generate a high-voltage tuning signal in a low-voltage system. Page 20.

High-Performance Difference Amplifier with Precision Supply-Referenced Level Shift

Designed on small-geometry processes, high-performance ADCs typically run on single 1.8-V to 5-V supplies. When processing ± 10 -V or larger signals, an amplifier circuit ahead of the ADC can attenuate the signal to keep it from saturating the ADC inputs. A difference amplifier (diff amp) is commonly used when the signal includes a large common-mode voltage. Page 23.

Dan Sheingold [dan.sheingold@analog.com]

Scott Wayne [scott.wayne@analog.com]

PRODUCT INTRODUCTIONS: VOLUME 44, NUMBER 4

Data sheets for all ADI products can be found by entering the part number in the search box at www.analog.com.

October

Amplifier, difference, high-voltage, zero-drift AD8207
DAC, voltage-output, 20-bit, ± 1 -LSB INL AD5791
Driver, backlight, 7-channel, charge pump ADP8870
Driver, current, programmable, industrial AD5749
Driver, MOSFET, dual, high-speed, 4-A ADP3654
Multiplexer, CMOS, 4-channel, differential ADG5409
Multiplexer, CMOS, 4-channel, latch-up proof ADG5404
Multiplexer, CMOS, 8-channel, latch-up proof ADG5408
Sensor, angular rate, precision ADIS16133
Transceiver, FSK/GFSK/OOK/MSK/GMSK ADF7023
Translator, clock, integer-N AD9550
Transmitter, HDMI, low-power, CEC ADV7524A

November

ADC, pipelined, 14-bit, 80-MSPS AD9641
ADC, SAR, 8-channel, 12-bit, 1-MSPS AD7298
Amplifier, audio, Class-D, 3-W mono SSM2375
Amplifiers, thermocouple, with CJC AD849x
Controller, hot-swap/digital power monitor ADM1275
Regulators, low-dropout, 150-mA loads ADP160/ADP162

December

ADC, pipelined, 16-bit, 200-MSPS/250-MSPS AD9467
ADC, SAR, 8-channel, 10-bit, 1-MSPS AD7298-1
Amplifier, audio, Class-D, 2 \times 2-W stereo SSM2380
Amplifier, audio, Class-D, 2.4-W mono, digital-input SSM2517
Amplifier, difference, pin-selectable attenuation AD8475
Amplifier, variable-gain, digitally programmable, dual AD8366
Codec, audio, 28-/56-bit, 2 ADCs/2 DACs ADAU1961
Comparator, fast, low-power, automotive-grade AD8468
Converter, dc-to-dc, 6-MHz, step-down, 500-mA ADP2125
Converter, dc-to-dc, isolated, 5 kV rms ADuM6000
DACs, octal, 12-/16-bit, 5-ppm/ $^{\circ}$ C reference AD5629R/AD5669R
DACs, unbuffered-voltage output,
12-/16-bit, 1- μ s AD5512A/AD5542A
Drivers, ADC, ultralow-noise ADA4930-x
Front Ends, analog, 8-channel, medical/auto AD9278/AD9279
Generator, clock, low-jitter, 14-output/29-output AD9523-1
Isolators, digital, 2-channel, 5-kV rms ADuM2210/ADuM2211
Isolators, digital, 2-channel, 5-kV, 400-mW dc-to-dc ADuM620x
Isolators, digital, 4-channel, transformer driver ADuM347x
Microcontroller, precision analog, ARM7, 12-bit ADuC7126
Mixer, balanced, 2200-MHz to 2700-MHz ADL5353
Receiver, broadband, 100-MHz to 1000-MHz ADRF6850
Regulators, low-dropout, triple-output, 200-mA ... ADP322/ADP323
Sensor, inertial, six-degrees-of-freedom ADIS16375
Sensor, vibration, digital, 3-axis ADIS16227
Supervisors, microprocessor,
programmable 2-supply ADM6305/ADM6306
Switches, CMOS, quad SPST,
power-off protection ADG4612/ADG4613
Switches, CMOS, triple/quad SPDT,
latch-up proof ADG5433/ADG5434
Transistors, matched, quad NPN MAT14

Analog Dialogue

Analog Dialogue, www.analog.com/analogdialogue, the technical magazine of Analog Devices, discusses products, applications, technology, and techniques for analog, digital, and mixed-signal processing. Published continuously for 44 years—starting in 1967—it is currently available in two versions. Monthly editions offer technical articles; timely information including recent application notes, new-product briefs, pre-release products, webinars and tutorials, and published articles; and potpourri, a universe of links to important and relevant information on the Analog Devices website, www.analog.com. Printable quarterly issues feature collections of monthly articles. For history buffs, the *Analog Dialogue* archive includes all regular editions, starting with Volume 1, Number 1 (1967), and three special anniversary issues. If you wish to subscribe, please go to www.analog.com/analogdialogue/subscribe.html. Your comments are always welcome; please send messages to dialogue.editor@analog.com or to Dan Sheingold, Editor [dan.sheingold@analog.com] or Scott Wayne, Publisher and Managing Editor [scott.wayne@analog.com].

Two Ways to Measure Temperature Using Thermocouples Feature Simplicity, Accuracy, and Flexibility

By Matthew Duff and Joseph Towe

Introduction

The thermocouple is a simple, widely used component for measuring temperature. This article provides a basic overview of thermocouples, describes common challenges encountered when designing with them, and suggests two signal conditioning solutions. The first solution combines both reference-junction compensation and signal conditioning in a single analog IC for convenience and ease of use; the second solution separates the reference-junction compensation from the signal conditioning to provide digital-output temperature sensing with greater flexibility and accuracy.

Thermocouple Theory

A thermocouple, shown in Figure 1, consists of two wires of dissimilar metals joined together at one end, called the *measurement* (“hot”) junction. The other end, where the wires are not joined, is connected to the signal conditioning circuitry traces, typically made of copper. This junction between the thermocouple metals and the copper traces is called the *reference* (“cold”) junction.*

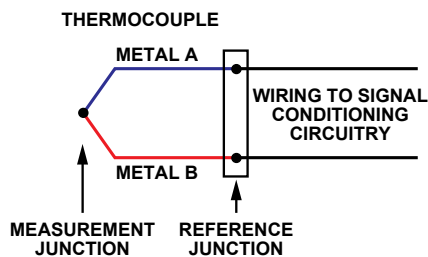


Figure 1. Thermocouple.

The voltage produced at the reference junction depends on the temperatures at both the measurement junction and the reference junction. Since the thermocouple is a differential device rather than an absolute temperature measurement device, the reference junction temperature must be known to get an accurate absolute temperature reading. This process is known as reference junction compensation (cold junction compensation.)

Thermocouples have become the industry-standard method for cost-effective measurement of a wide range of temperatures with reasonable accuracy. They are used in a variety of applications up to approximately +2500°C in boilers, water heaters, ovens, and aircraft engines—to name just a few. The most popular thermocouple is the type K, consisting of Chromel® and Alumel® (trademarked nickel alloys containing *chromium*, and *aluminum*, manganese, and silicon, respectively), with a measurement range of –200°C to +1250°C.

*We use the terms “measurement junction” and “reference junction” rather than the more traditional “hot junction” and “cold junction.” The traditional naming system can be confusing because in many applications the measurement junction can be colder than the reference junction.

Why Use a Thermocouple?

Advantages

- **Temperature range:** Most practical temperature ranges, from cryogenics to jet-engine exhaust, can be served using thermocouples. Depending on the metal wires used, a thermocouple is capable of measuring temperature in the range –200°C to +2500°C.
- **Robust:** Thermocouples are rugged devices that are immune to shock and vibration and are suitable for use in hazardous environments.
- **Rapid response:** Because they are small and have low thermal capacity, thermocouples respond rapidly to temperature changes, especially if the sensing junction is exposed. They can respond to rapidly changing temperatures within a few hundred milliseconds.
- **No self heating:** Because thermocouples require no excitation power, they are not prone to self heating and are intrinsically safe.

Disadvantages

- **Complex signal conditioning:** Substantial signal conditioning is necessary to convert the thermocouple voltage into a usable temperature reading. Traditionally, signal conditioning has required a large investment in design time to avoid introducing errors that degrade accuracy.
- **Accuracy:** In addition to the inherent inaccuracies in thermocouples due to their metallurgical properties, a thermocouple measurement is only as accurate as the reference junction temperature can be measured, traditionally within 1°C to 2°C.
- **Susceptibility to corrosion:** Because thermocouples consist of two dissimilar metals, in some environments corrosion over time may result in deteriorating accuracy. Hence, they may need protection; and care and maintenance are essential.
- **Susceptibility to noise:** When measuring microvolt-level signal changes, noise from stray electrical and magnetic fields can be a problem. Twisting the thermocouple wire pair can greatly reduce magnetic field pickup. Using a shielded cable or running wires in metal conduit and guarding can reduce electric field pickup. The measuring device should provide signal filtering, either in hardware or by software, with strong rejection of the line frequency (50 Hz/60 Hz) and its harmonics.

Difficulties Measuring with Thermocouples

It is not easy to transform the voltage generated by a thermocouple into an accurate temperature reading for many reasons: the voltage signal is small, the temperature-voltage relationship is nonlinear, reference junction compensation is required, and thermocouples may pose grounding problems. Let’s consider these issues one by one.

Voltage signal is small: The most common thermocouple types are J, K, and T. At room temperature, their voltage varies at 52 $\mu\text{V}/^\circ\text{C}$, 41 $\mu\text{V}/^\circ\text{C}$, and 41 $\mu\text{V}/^\circ\text{C}$, respectively. Other less-common types have an even smaller voltage change with temperature. This small signal requires a high gain stage before analog-to-digital conversion. Table 1 compares sensitivities of various thermocouple types.

Table 1. Voltage Change vs. Temperature Rise (Seebeck Coefficient) for Various Thermocouple Types at 25°C.

Thermocouple Type	Seebeck Coefficient ($\mu\text{V}/^\circ\text{C}$)
E	61
J	52
K	41
N	27
R	9
S	6
T	41

Because the voltage signal is small, the signal-conditioning circuitry typically requires gains of about 100 or so—fairly straightforward signal conditioning. What can be more difficult is distinguishing the actual signal from the noise picked up on the thermocouple leads. Thermocouple leads are long and often run through electrically noisy environments. The noise picked up on the leads can easily overwhelm the tiny thermocouple signal.

Two approaches are commonly combined to extract the signal from the noise. The first is to use a differential-input amplifier, such as an instrumentation amplifier, to amplify the signal. Because much of the noise appears on both wires (*common-mode*), measuring differentially eliminates it. The second is low-pass filtering, which removes out-of-band noise. The low-pass filter should remove both radio-frequency interference (above 1 MHz) that may cause rectification in the amplifier and 50 Hz/60 Hz (power-supply) *hum*. It is important to place the filter for radio frequency interference ahead of the amplifier (or use an amplifier with filtered inputs). The location of the 50-Hz/60-Hz filter is often not critical—it can be combined with the RFI filter, placed between the amplifier and ADC, incorporated as part of a sigma-delta ADC, or it can be programmed in software as an averaging filter.

Reference junction compensation: The temperature of the thermocouple’s reference junction must be known to get an accurate absolute-temperature reading. When thermocouples were first used, this was done by keeping the reference junction in an ice bath. Figure 2 depicts a thermocouple circuit with one end at an unknown temperature and the other end in an ice bath (0°C). This method was used to exhaustively characterize the various thermocouple types, thus almost all thermocouple tables use 0°C as the reference temperature.

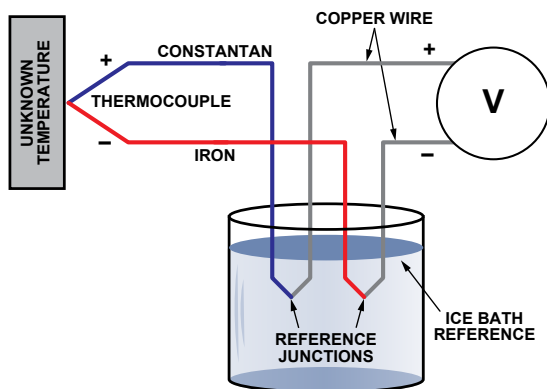


Figure 2. Basic iron-constantan thermocouple circuit.

But keeping the reference junction of the thermocouple in an ice bath is not practical for most measurement systems. Instead most systems use a technique called *reference-junction compensation*, (also known as *cold-junction compensation*). The reference junction temperature is measured with another temperature-sensitive device—typically an IC, thermistor, diode, or RTD

(resistance temperature-detector). The thermocouple voltage reading is then compensated to reflect the reference junction temperature. It is important that the reference junction be read as accurately as possible—with an accurate temperature sensor kept at the same temperature as the reference junction. Any error in reading the reference junction temperature will show up directly in the final thermocouple reading.

A variety of sensors are available for measuring the reference temperature:

1. Thermistors: They have fast response and a small package; but they require linearization and have limited accuracy, especially over a wide temperature range. They also require current for excitation, which can produce self-heating, leading to drift. Overall system accuracy, when combined with signal conditioning, can be poor.
2. Resistance temperature-detectors (RTDs): RTDs are accurate, stable, and reasonably linear, however, package size and cost restrict their use to process-control applications.
3. Remote thermal diodes: A diode is used to sense the temperature near the thermocouple connector. A conditioning chip converts the diode voltage, which is proportional to temperature, to an analog or digital output. Its accuracy is limited to about $\pm 1^\circ\text{C}$.
4. Integrated temperature sensor: An integrated temperature sensor, a standalone IC that senses the temperature locally, should be carefully mounted close to the reference junction, and can combine reference junction compensation and signal conditioning. Accuracies to within small fractions of 1°C can be achieved.

Voltage signal is nonlinear: The slope of a thermocouple response curve changes over temperature. For example, at 0°C, a T-type thermocouple output changes at $39 \mu\text{V}/^\circ\text{C}$, but at 100°C, the slope increases to $47 \mu\text{V}/^\circ\text{C}$.

There are three common ways to compensate for the nonlinearity of the thermocouple.

Choose a portion of the curve that is relatively flat and approximate the slope as linear in this region—an approach that works especially well for measurements over a limited temperature range. No complicated computations are needed. One of the reasons the K- and J-type thermocouples are popular is that they both have large stretches of temperature for which the incremental slope of the sensitivity (Seebeck coefficient) remains fairly constant (see Figure 3).

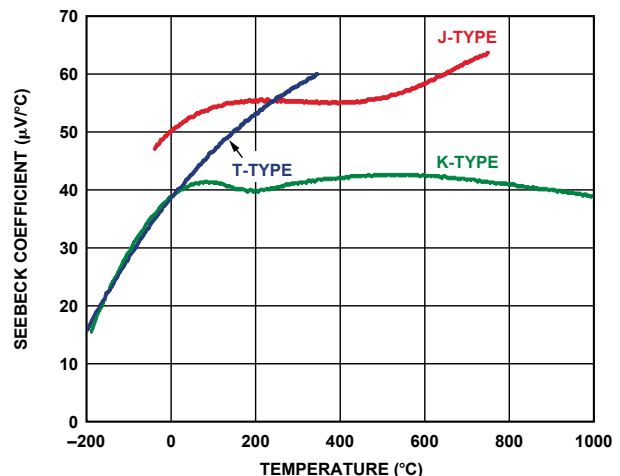


Figure 3. Variation of thermocouple sensitivity with temperature. Note that K-type’s Seebeck coefficient is roughly constant at about $41 \mu\text{V}/^\circ\text{C}$ from 0°C to 1000°C.

Another approach is to store in memory a lookup table that matches each of a set of thermocouple voltages to its respective temperature. Then use linear interpolation between the two closest points in the table to get other temperature values.

A third approach is to use higher order equations that model the behavior of the thermocouple. While this method is the most accurate, it is also the most computationally intensive. There are two sets of equations for each thermocouple. One set converts temperature to thermocouple voltage (useful for reference junction compensation). The other set converts thermocouple voltage to temperature. Thermocouple tables and the higher order thermocouple equations can be found at <http://srdata.nist.gov/its90/main/>. The tables and equations are all based on a reference-junction temperature of 0°C. Reference-junction compensation must be used if the reference-junction is at any other temperature.

Grounding requirements: Thermocouple manufacturers make thermocouples with both insulated and grounded tips for the measurement junction (Figure 4).

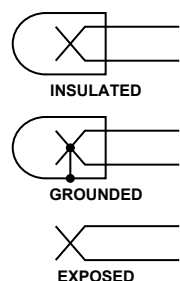


Figure 4. Thermocouple measurement junction types.

The thermocouple signal conditioning should be designed so as to avoid ground loops when measuring a grounded thermocouple, yet also have a path for the amplifier input bias currents when measuring an insulated thermocouple. In addition, if the thermocouple tip is grounded, the amplifier input range should be designed to handle any differences in ground potential between the thermocouple tip and the measurement system ground (Figure 5).

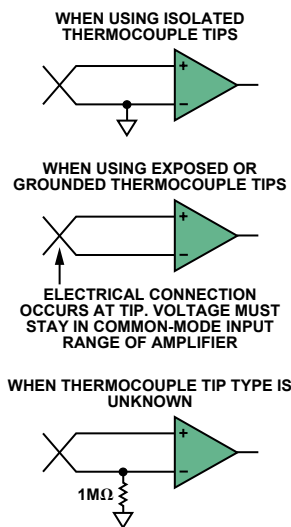


Figure 5. Grounding options when using different tip types.

For nonisolated systems, a dual-supply signal-conditioning system will typically be more robust for grounded tip and exposed tip types. Because of its wide common-mode input range, a dual-supply amplifier can handle a large voltage differential between the PCB (printed-circuit board) ground and the ground at the thermocouple tip. Single-supply systems can work satisfactorily in

all three tip cases if the amplifier's common-mode range has some ability to measure below ground in the single-supply configuration. To deal with the common-mode limitation in some single-supply systems, biasing the thermocouple to a midscale voltage is useful. This works well for insulated thermocouple tips, or if the overall measurement system is isolated. However, it is not recommended for nonisolated systems that are designed to measure grounded or exposed thermocouples.

Practical thermocouple solutions: Thermocouple signal conditioning is more complex than that of other temperature measurement systems. The time required for the design and debugging of the signal conditioning can increase a product's time to market. Errors in the signal conditioning, especially in the reference junction compensation section, can lead to lower accuracy. The following two solutions address these concerns.

The first details a simple analog integrated hardware solution combining direct thermocouple measurement with reference-junction compensation using a single IC. The second solution details a software-based reference-junction compensation scheme providing improved accuracy for the thermocouple measurement and the flexibility to use many types of thermocouples.

Measurement Solution 1: Optimized for Simplicity

Figure 6 shows a schematic for measuring a K-type thermocouple. It is based on using the AD8495 thermocouple amplifier, which is designed specifically to measure K-type thermocouples. This analog solution is optimized for minimum design time: It has a straightforward signal chain and requires no software coding.

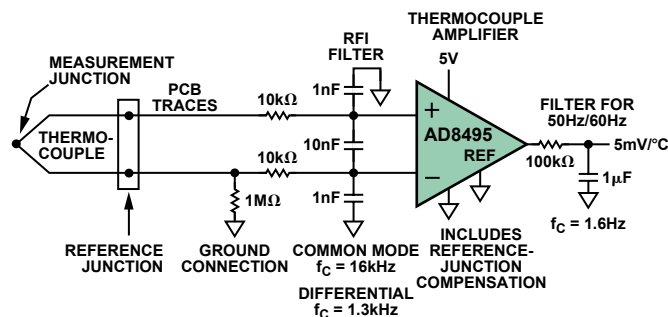


Figure 6. Measurement Solution 1: optimized for simplicity.

How does this simple signal chain address the signal conditioning requirements for K-type thermocouples?

Gain and output scale factor: The small thermocouple signal is amplified by the AD8495's gain of 122, resulting in a 5-mV/°C output signal sensitivity (200°C/V).

Noise reduction: High-frequency common-mode and differential noise are removed by the external RFI filter. Low frequency common-mode noise is rejected by the AD8495's instrumentation amplifier. Any remaining noise is addressed by the external post filter.

Reference-junction compensation: The AD8495, which includes a temperature sensor to compensate for changes in ambient temperature, must be placed near the reference junction to maintain both at the same temperature for accurate reference-junction compensation.

Nonlinearity correction: The AD8495 is calibrated to give a 5 mV/°C output on the linear portion of the K-type thermocouple curve, with less than 2°C of linearity error in the -25°C to +400°C temperature range. If temperatures beyond this range are needed, Analog Devices Application Note AN-1087 describes how a lookup table or equation could be used in a microprocessor to extend the temperature range.

Table 2. Solution 1 (Figure 6) Performance Summary

Thermocouple Type	Measurement-Junction Temperature Range	Reference-Junction Temperature Range	Accuracy at 25°C	Power Consumption
K	-25°C to +400°C	0°C to 50°C	±3°C (A grade) ±1°C (C grade)	1.25 mW

Handling insulated, grounded, and exposed thermocouples:

Figure 5 shows a 1-MΩ resistor connected to ground, which allows for all thermocouple tip types. The AD8495 was specifically designed to be able to measure a few hundred millivolts below ground when used with a single supply as shown. If a larger ground differential is expected, the AD8495 can also be operated with dual supplies.

More about the AD8495: Figure 7 shows a block diagram of the AD8495 thermocouple amplifier. Amplifiers A1, A2, and A3—and the resistors shown—form an instrumentation amplifier that amplifies the K-type thermocouple’s output with a gain appropriate to produce an output voltage of 5 mV/°C. Inside the box labeled “Ref junction compensation” is an ambient temperature sensor. With the measurement junction temperature held constant, the differential voltage from the thermocouple will decrease if the reference junction temperature rises for any reason. If the tiny (3.2 mm × 3.2 mm × 1.2 mm) AD8495 is in close thermal proximity to the reference junction, the reference-junction compensation circuitry injects additional voltage into the amplifier, so that the output voltage stays constant, thus compensating for the reference temperature change.

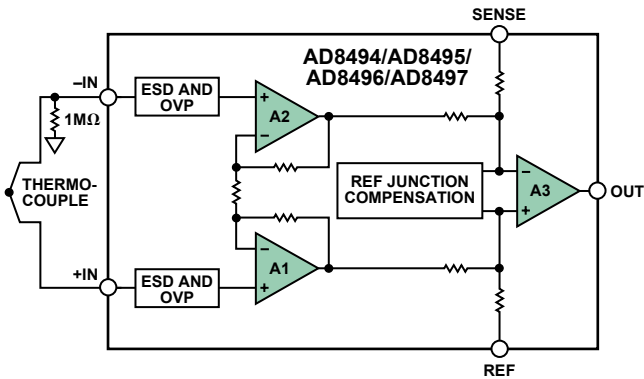


Figure 7. AD8495 functional block diagram.

Table 2 summarizes the performance of the integrated hardware solution using the AD8495:

Measurement Solution 2: Optimized for Accuracy and Flexibility

Figure 8 shows a schematic for measuring a J-, K-, or T-type thermocouple with a high degree of accuracy. This circuit includes a high-precision ADC to measure the small-signal thermocouple voltage and a high-accuracy temperature sensor to measure the reference-junction temperature. Both devices are controlled using an SPI interface from an external microcontroller.

How does this configuration address the signal conditioning requirements mentioned earlier?

Remove noise and amplify voltage: The AD7793, shown in detail in Figure 9—a high-precision, low-power analog front end—is used to measure the thermocouple voltage. The thermocouple output is filtered externally and connects to a set of differential inputs, AIN1(+) and AIN1(-). The signal is then routed through a multiplexer, a buffer, and an instrumentation amplifier—which amplifies the small thermocouple signal—and to an ADC, which converts the signal to digital.

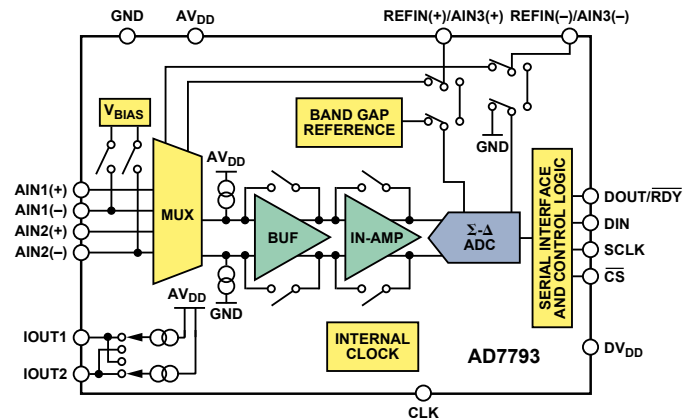


Figure 9. AD7793 functional block diagram.

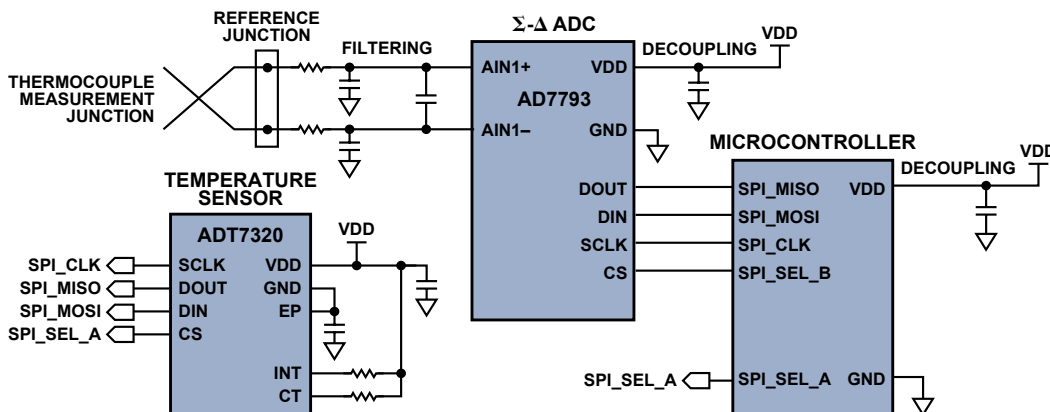


Figure 8. Measurement Solution 2: Optimized for accuracy and flexibility.

Table 3. Solution 2 (Figure 8) Performance Summary

Thermocouple Type	Measurement-Junction Temperature Range	Reference-Junction Temperature Range	Accuracy	Power Consumption
J, K, T	Full Range	-10°C to +85°C -20°C to +105°C	±0.2°C ±0.25°C	3 mW 3 mW

Compensate for reference-junction temperature:

The ADT7320 (detailed in Figure 10), if placed close enough to the reference junction, can measure the reference-junction temperature accurately, to ±0.2°C, from -10°C to +85°C. An on-chip temperature sensor generates a voltage proportional to absolute temperature, which is compared to an internal voltage reference and applied to a precision digital modulator. The digitized result from the modulator updates a 16-bit temperature value register. The temperature value register can then be read back from a microcontroller, using an SPI interface, and combined with the temperature reading from the ADC to effect the compensation.

Correct nonlinearity: The ADT7320 provides excellent linearity over its entire rated temperature range (-40°C to +125°C), requiring no correction or calibration by the user. Its digital output can thus be considered an accurate representation of the reference-junction state.

To determine the actual thermocouple temperature, this reference-temperature measurement must be converted into an equivalent thermoelectric voltage using equations provided by the National Institute of Standards and Technology (NIST). This voltage then gets added to the thermocouple voltage measured by the AD7793; and the summation is then translated back into a thermocouple temperature, again using NIST equations.

Handle insulated and grounded thermocouples: Figure 8 shows a thermocouple with an exposed tip. This provides the best response time, but the same configuration could also be used with an insulated-tip thermocouple.

Table 3 summarizes the performance of the software-based reference-junction measurement solution, using NIST data:

Conclusion

Thermocouples offer robust temperature measurement over a quite wide temperature range, but they are often not a first choice for temperature measurement because of the required trade-offs between design time and accuracy. This article proposes cost-effective ways of resolving these concerns.

The first solution concentrates on reducing the complexity of the measurement by means of a hardware-based analog reference-junction compensation technique. It results in a straightforward signal chain with no software programming required, relying on the integration provided by the AD8495 thermocouple amplifier, which produces a 5-mV/°C output signal that can be fed into the analog input of a wide variety of microcontrollers.

The second solution provides the highest accuracy measurement and also enables the use of various thermocouple types. A software-based reference-junction compensation technique, it relies on the high-accuracy ADT7320 digital temperature sensor to provide a much more accurate reference-junction compensation measurement than had been achievable until now. The ADT7320 comes fully calibrated and specified over the -40°C to +125°C temperature range. Completely transparent, unlike a traditional thermistor or RTD sensor measurement, it neither requires a costly calibration step after board assembly, nor does it consume processor or memory resources with calibration coefficients or linearization routines. Consuming only microwatts of power, it avoids self-heating issues that undermine the accuracy of traditional resistive sensor solutions.

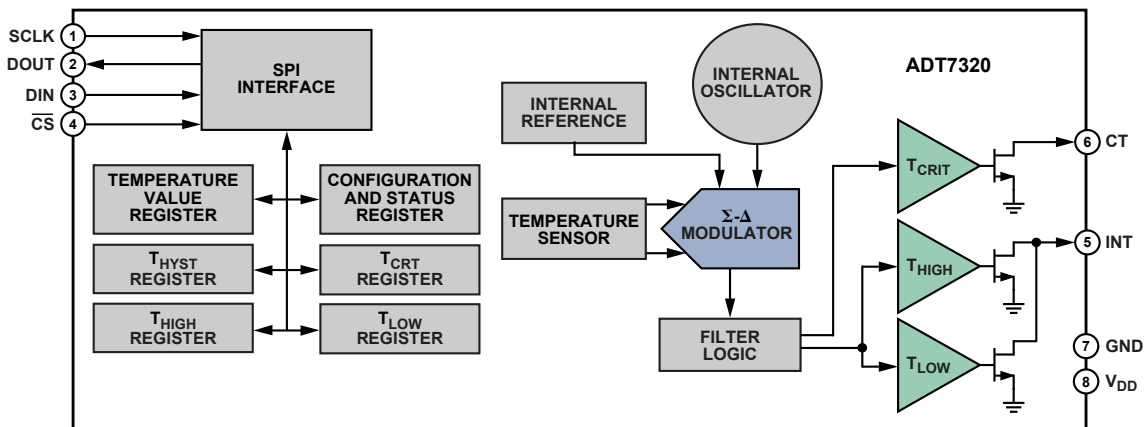


Figure 10. ADT7320 functional block diagram.

Appendix

Use of NIST Equation to Convert ADT7320 Temperature to Voltage

The thermocouple reference-junction compensation is based on the relationship:

$$\Delta V = V @ J_1 - V @ J_2 \quad (1)$$

where:

ΔV = thermocouple output voltage

$V @ J_1$ = voltage generated at the thermocouple junction

$V @ J_2$ = voltage generated at the reference junction

For this compensation relationship to be valid, both terminals of the reference junction must be maintained at the same temperature. Temperature equalization is accomplished with an isothermal terminal block that permits the temperature of both terminals to equalize while maintaining electrical isolation.

After the reference-junction temperature is measured, it must be converted into the equivalent thermoelectric voltage that would be generated with the junction at the measured temperature. One technique uses a power series polynomial. The thermoelectric voltage is calculated:

$$E = a_0 + a_1T + a_2T^2 + a_3T^3 + \dots + a_nT^n \quad (2)$$

where:

E = thermoelectric voltage (microvolts)

a_n = thermocouple-type-dependent polynomial coefficients

T = temperature (°C)

n = order of polynomial

NIST publishes tables of polynomial coefficients for each type of thermocouple. In these tables are lists of coefficients, order (the number of terms in the polynomial), valid temperature ranges for each list of coefficients, and error range. Some types of thermocouples require more than one table of coefficients to cover the entire temperature operating range. Tables for the power series polynomial are listed in the main text.

Authors

Matthew Duff [matthew.duff@analog.com]

joined Analog Devices in 2005 as an applications engineer in the Integrated Amplifier Products Group. Prior to joining Analog Devices, Matt worked for National Instruments in both design and project management positions on instrumentation and automotive products. He received his BS from Texas A&M and MS from Georgia Tech, both in electrical engineering.



Joseph Towey [joe.towey@analog.com]

joined Analog Devices in 2002 as a senior test development engineer with the Thermal Sensing Group. Joe is currently applications manager for the Thermal Sensing and Switch/Multiplexer Group. Prior to joining Analog Devices, Joe worked for Tellabs and Motorola in both test development and project management positions. He is qualified with a BSc (Hons) degree in computer science and a diploma in electronic engineering.



Inertial Sensors Facilitate Autonomous Operation in Mobile Robots

By Mark Looney

Introduction

Ground-based robot systems must often handle “the dull, the dirty, and the dangerous” tasks, according to Seth Allen, project manager at [Adept MobileRobots](#).¹ In other words, robot systems are typically used for missions where direct human involvement is too expensive, too dangerous, or just ineffective. In many cases, the ability of robotic platforms to operate autonomously is a valuable feature, using navigation systems to monitor and control their motion when moving from one location to the next. Accuracy in managing position and motion is a key factor in enabling really useful autonomous operation, and MEMS (*microelectromechanical system*) gyroscopes provide a feedback sensing mechanism that can be very useful in optimizing navigation system performance. The Seekur[®] robot system, shown in Figure 1, is an example of an autonomous system that employs advanced MEMS devices to improve navigation performance.



Figure 1. Adept MobileRobots Seekur system.

Robot Navigation Overview

A robot movement typically starts with a position change request from the central processor that is managing the progress of the robot’s overall mission. The *navigation system* begins executing a position change request by developing a trip plan or trajectory. The trip plan considers available paths, known obstacle locations, robot capability, and any relevant mission objectives. (For example, delivery time can be critical for a specimen delivery robot in a hospital.) The trip plan is fed into a controller, which produces drive and direction profiles for navigational control. These profiles result in motion and progress with respect to the plan. The motion is typically monitored by a number of sensing systems, each of which produces feedback signals; the feedback controller combines and translates them into updated trip plans and conditions. Figure 2 is a basic block diagram of a generic navigation system.

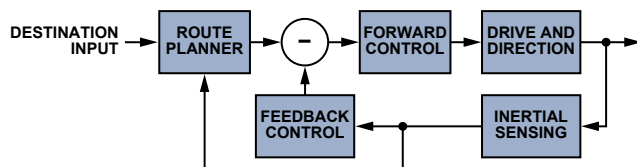


Figure 2. Generic navigation system.

The key steps in developing a navigation system start with a good understanding of each function, with particular emphasis on its operational goals and limitations. Each function typically has some clearly defined and easily executed aspects, but also offers challenging limitations that need to be managed. In some cases, this process can be iterative, where identifying and dealing with limitations enables new opportunities for optimization. The best way to describe this process is through an example.

Adept MobileRobots Seekur

The [Adept MobileRobots Seekur](#)² is an autonomous robot that uses an *inertial navigation system* (INS) similar to the one shown in Figure 3. This vehicle has a 4-wheel drive system, with independent steering and speed control for each wheel, providing the flexibility to move the platform in any horizontal direction. This ability is valuable for robotic vehicles in such emerging applications as warehouse delivery systems, hospital specimen/supply delivery systems, and military force augmentation systems.

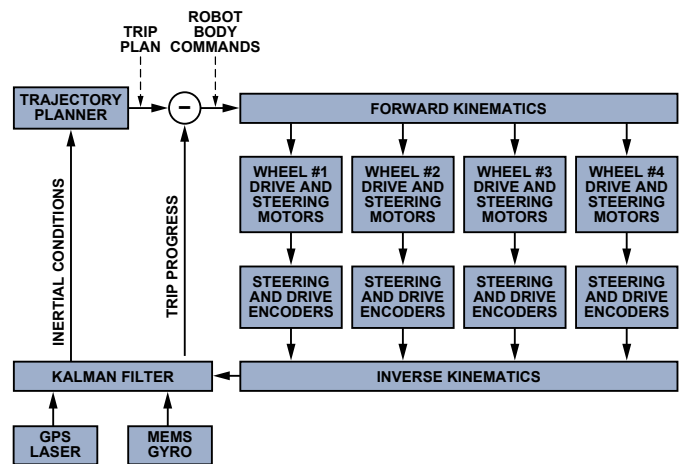


Figure 3. Adept MobileRobots Seekur navigation system.

Forward Control

Robot body commands, the main *error signals*, represent the difference between the trip plan provided by the trajectory planner and *trip progress* updates produced by the feedback sensing system. They are fed into the *inverse kinematics* system, which translates the robot body commands into steering and velocity profiles for each individual wheel. These profiles are calculated using *Ackermann steering relationships*,* which incorporate tire diameter, surface contact area, spacing, and other important geometrical features. Ackermann steering principles and relationships enable these robot platforms to create electronically linked steering angle profiles similar to those of the mechanical rack-and-pinion systems used in many automotive steering systems. Incorporating these relationships remotely, without requiring the axles to be mechanically linked, helps minimize friction and tire slip, provides the benefits of reduced tire wear and energy loss, and allows motion not possible with simple mechanical linkages.

Wheel Drive and Steering System

Each wheel has a *drive shaft* that is mechanically coupled to its drive motor through a gear box and—through another gear box—to an optical encoder, which is an input to the *odometry feedback* system. The *steering shaft* couples the axle to another servo motor, which establishes the wheel’s steering angle. The steering shaft also couples to a second optical encoder through a gear box—which provides another input to the odometry feedback system.

*Patented by Rudolph Ackermann in 1817(!)

Feedback Sensing and Control

The navigation system uses an extended [Kalman filter](#)³ to estimate the pose of the robot on the map by combining data from multiple sensors. The odometry data on the Seekur is derived from the wheel traction and steering encoders—which provide the translation—and a MEMS gyro, which provides the rotation.

Odometry

The odometry feedback system estimates robot position, heading, and speed using optical-encoder measurements of drive- and steering shaft rotation. In optical encoders, a disk blocks an internal light source or allows it to shine on a light sensor via thousands of tiny openings. As the disk rotates, it produces a series of electrical pulses that are typically fed into a counter circuit. The number of counts per rotation is equal to the number of slots in the disc, which allows the number of rotations (including fractional) to be calculated from the encoder circuit's pulse count. Figure 4 provides a graphical reference and relationship for translating the drive shaft's rotation count into linear *displacement* (position) changes.

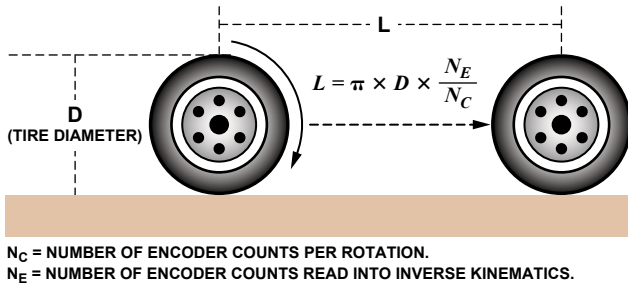


Figure 4. Odometry linear-displacement relationship.

The drive-axle and steering-shaft encoder measurements for each wheel are combined in the *forward-kinematics* processor, using the Ackermann steering formulas, which produce heading, turn rate, position, and linear velocity measurements.

The advantage of this measurement system is that its sensing function is directly coupled to the drive and steering control systems, so their state is accurately known. However, its accuracy in terms of the actual speed and direction of the vehicle is limited unless reference to a set of real-world coordinates is available. The primary limitations, or error sources, are in the tire-geometry consistency (the accuracy and variation of D in Figure 4) and breaks in the contact between the tire and the ground surface. Tire geometry is dependent on tread consistency, air pressure, temperature, and weight—all conditions that can change during normal robot use. Tire slip depends on turn radii, velocity, and surface consistency.

Position Sensing

The Seekur system uses various range sensors. For *indoor* applications, it employs a 270° laser scanner to build a map of its environment. The laser system measures object shapes, sizes, and distance from the laser source using returned-energy patterns and signal-return times. When in its mapping mode, it characterizes its workspace by combining scan results from many different positions in the workspace (Figure 5). This produces a map of object locations, sizes, and shapes, which is used as a reference for run-time scans. When used in conjunction with the mapping information, the laser scanner function provides accurate position information. If used by itself, it would bear limitations that include the stop time for scans and an inability to manage a changing environment. In a warehouse environment, people, lift trucks, pallet jacks, and many other objects change position often, which could potentially impact speed to a destination and, indeed, accuracy of achieving the correct destination.

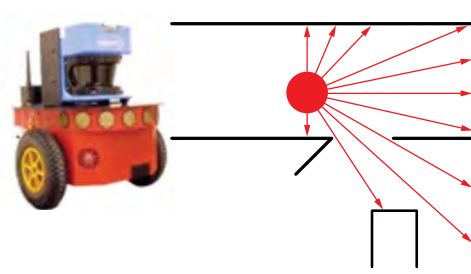


Figure 5. Laser mapping.

For *outdoor* applications, the Seekur uses *global positioning systems* (GPS) for position measurements (Figure 6). These systems use flight times of radio signals from at least four satellites to triangulate a position on the earth's surface. When available, they can provide levels of accuracy to within 1 m. However, these systems are limited by the *line of sight* requirements, which can be impeded by buildings, trees, bridges, tunnels, and many other types of objects. In some cases, where outdoor object locations and features are known (urban canyons), radar and sonar can also be used to supplement the position estimates during GPS outages. Even so, effectiveness is often limited when dynamic conditions exist, such as cars passing by or construction.

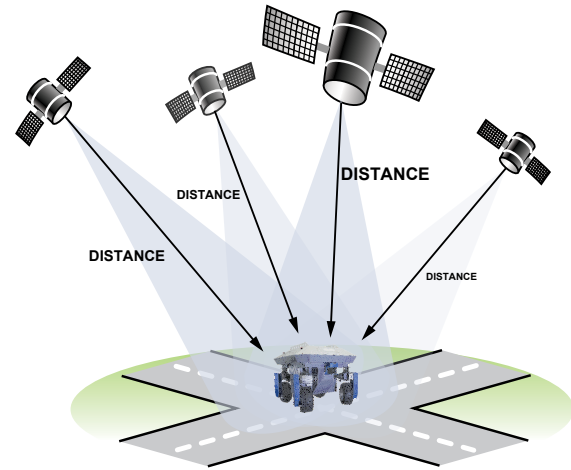


Figure 6. GPS position sensing.

MEMS Angular Rate Sensing

The MEMS gyroscope used in the Seekur system provides a direct measurement of the Seekur's rate of rotation about the yaw (vertical) axis, which is normal to the earth's surface in the Seekur navigational reference frame. The mathematical relationship for calculating a relative heading is a simple integration of the angular rate measurement over a fixed period (t_1 to t_2).

$$\theta_H = \int_{t_1}^{t_2} \omega \cdot dt$$

One of the key advantages of this approach is that the gyroscope, being attached to the robot frame, measures the vehicle's actual motion without relying on gear ratios, backlash, tire geometry, or surface contact integrity. However, the heading estimate does rely on sensor accuracy, which is a function of the following key parameters: bias error, noise, stability, and sensitivity. Fixed bias error translates into a heading drift rate, as shown in the following relationship that includes the bias error, ω_{BE} :

$$\theta_H = \int_{t_1}^{t_2} (\omega + \omega_{BE}) \cdot dt = \int_{t_1}^{t_2} \omega \cdot dt + \underline{\underline{(t_2 - t_1) \cdot \omega_{BE}}}$$

Bias error can be broken down into two categories: *current* and *condition-dependent*. The Seekur system estimates current bias errors when it is not in motion. This requires the navigation computer to recognize when no position change commands are being executed and facilitate data-collection bias estimate and correction-factor updates. The accuracy of this process depends on sensor noise and the amount of time available to collect data and formulate an error estimate. The *Allan variance curve* provides a convenient relationship between bias accuracy and averaging time, as shown in Figure 7, which captures the relationship for the ADIS16265—an iSensor® MEMS device similar to the gyroscope currently used in the Seekur system. In this case, the Seekur can reduce the bias error to less than 0.01°/sec, averaged over 20 seconds, and can optimize the estimate by averaging over about 100 seconds.

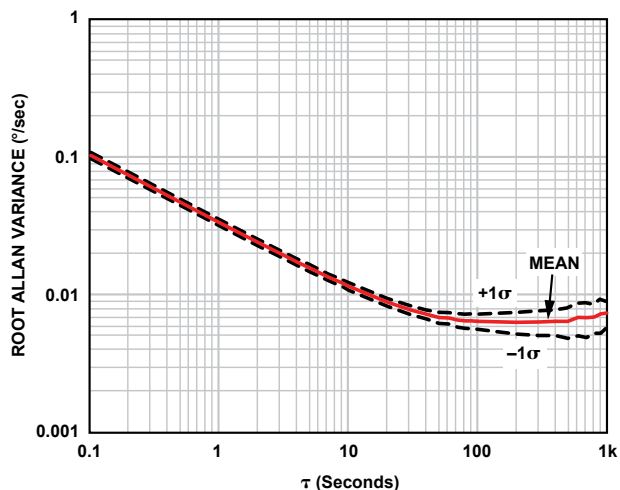


Figure 7. ADIS16265 Allan variance curve.

The Allan variance⁴ relationship also offers insights into the optimal integration time ($\tau = t_2 - t_1$). The minimum point on this curve is typically identified as the *in-run bias stability*. The heading estimates are optimized by setting the integration time, τ , equal to the integration time associated with the minimum point on the Allan variance curve for the gyroscope in use.

Because they influence performance, *condition-dependent* errors, such as bias temperature coefficient, can determine how often the robot must stop to update its bias correction. Using precalibrated sensors can help address the most common error sources, such as temperature- and power-supply changes. For example, a change from the ADIS16060 to the precalibrated ADIS16265 may incrementally increase size, price, and power, but offers 18× better stability with respect to temperature. For a 2°C change in temperature, the maximum bias of 0.22°/sec with the ADIS16060 is reduced to 0.012°/sec with the ADIS16265.

The sensitivity error source is proportional to the actual change in heading, as shown in the following relationship:

$$\theta_H = \int_{t_1}^{t_2} (1 + \varepsilon) \cdot \omega \cdot dt = \int_{t_1}^{t_2} \omega \cdot dt + \int_{t_1}^{t_2} \varepsilon \cdot \omega \cdot dt$$

Commercial MEMS sensors often provide sensitivity error specifications that range from ±5% to above ±20%, so they will need calibration to minimize these errors. Precalibrated MEMS⁵ gyroscopes, such as the ADIS16265 and ADIS16135, provide specifications of less than ±1%—with even better performance in controlled environments.

Application Examples: Warehouse Inventory Delivery

Warehouse automation currently uses lift trucks and belt systems to move materials for organizing inventory and fulfilling demands. The lift trucks require direct human control, and the belt system requires regular maintenance attention. In order to achieve maximum warehouse value, many warehouses are being reconfigured, a process that opens the door for autonomous robot platforms. Instead of a substantial construction effort to revise lift trucks and belt systems, a fleet of robots requires only software changes and retraining the robot’s navigation system for its new mission. The key performance requirement in a warehouse delivery system is the robot’s ability to maintain a consistent pattern of travel and maneuver safely in a dynamic environment, where obstacles move and human safety cannot be compromised. In order to demonstrate the value of MEMS gyroscope feedback on the Seekur in this type of application, Adept MobileRobots conducted an experiment to find out how well the Seekur would maintain a repetitive path, without (Figure 8) and with (Figure 9) MEMS gyroscopic feedback. It is important to note that this experiment was run without GPS or laser-scanning correction—for the purpose of studying the impact of MEMS gyroscopic feedback.

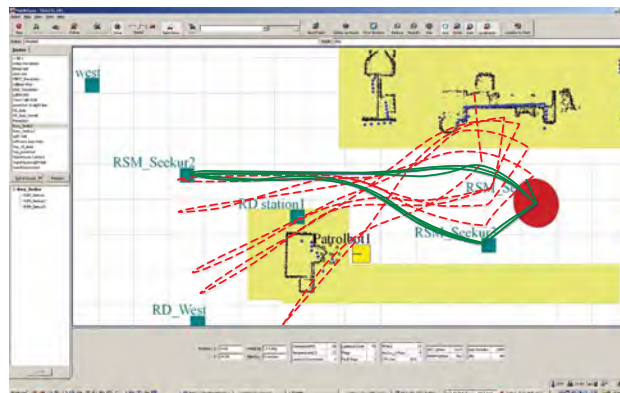


Figure 8. Seekur path accuracy, no MEMS gyroscope feedback.

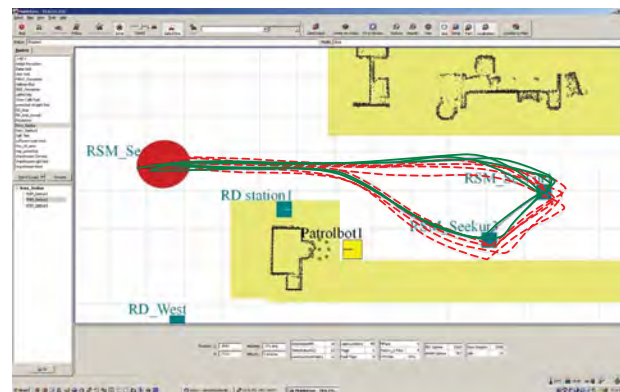


Figure 9. Seekur path accuracy, MEMS gyroscope feedback enabled.

The difference in maintaining the path accuracy is easy to see when comparing the path traces in Figure 8 and Figure 9. It is important to note that these experiments were run on early generation MEMS technology that supported ~0.02°/sec stability. Current gyroscopes enable 2× to 4× performance improvement at the same cost, size, and power levels. As this trend continues, the ability to maintain accurate navigation on repetitive paths will continue to improve—opening up additional markets and applications, such as specimen and supply delivery in hospitals.

Supply Convoys

Current DARPA initiatives continue to call for more robot technology to help in *force multiplication*. Supply convoys are an example of this type of application, where military convoys are exposed to opposing threats while forced to move in slow, predictable patterns. Accurate navigation enables robots, like the Seekur, to take on more responsibility in supply convoys, reducing human exposure to threats along their paths. One key performance metric, where the MEMS gyroscope heading feedback is particularly helpful, is in managing GPS outage conditions. The latest Seekur navigation effort, geared towards this environment, employs MEMS inertial measurement units (IMUs)⁶ for better accuracy and their ability to incorporate future integration advances—for terrain management and other functional areas.

In order to test how well this system localizes—with and without the IMU—the error of an outdoor path was recorded and analyzed. Figure 10 shows the comparison of the errors—with respect to the true path (from the GPS)—of the odometry only with the errors when the odometry and the IMU are combined in the Kalman filter. The positional accuracy was nearly 15× better in the latter case.

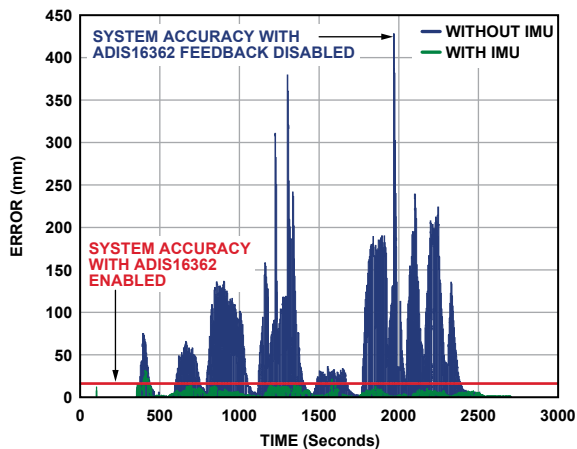


Figure 10. Seekur position error using odometry/IMU (green) vs. odometry only (blue).

Conclusion

Robot platform developers are finding that MEMS gyroscope technology provides cost-effective methods for improving directional estimation and overall accuracy in their navigation

systems. The availability of precalibrated, system-ready devices enables simple functional integration, which leads to early success in the development process and allows engineers to concentrate on system optimization. As MEMS technology continues to improve gyroscope noise, stability, and accuracy specifications, it will continue to enable higher levels of accuracy and control, which will likely continue to open new markets for autonomous robot platforms. Next-generation development for systems such as the Seekur could move from gyroscopes to fully integrated MEMS IMU/6-degrees-of-freedom (6DoF) sensors. While the yaw-oriented approach is useful, the world isn't flat; many other applications, existing and future, can incorporate MEMS IMUs for terrain management and for additional accuracy refinement, with three gyroscopes enabling full alignment feedback and correction.

Acknowledgment

Analog Devices would like to thank Seth Allen, George Paul, and the entire team at Adept MobileRobots for the contributions that they made to this article.

References

- (Information on all ADI components can be found at www.analog.com.)
- <http://go.adept.com/content/adeptacqmobrob06142010>.
 - www.mobilerobots.com/researchrobots/researchrobots/seekurugv.aspx.
 - http://en.wikipedia.org/wiki/Kalman_filter.
 - http://en.wikipedia.org/wiki/Allan_Variance.
 - www.analog.com/library/analogdialogue/archives/43-09/EDCh%203%20sensors.pdf.
 - www.analog.com/en/mems/imu/products/index.html.

Author

Mark Looney [mark.looney@analog.com] is an *i*Sensor applications engineer at Analog Devices in Greensboro, NC. Since joining ADI in 1998, he has accumulated experience in sensor signal processing, high-speed analog-to-digital converters, and dc-to-dc power conversion. He earned BS (1994) and MS (1995) degrees in electrical engineering from the University of Nevada, Reno, and has published several articles. Prior to joining ADI, he helped start IMATS, a vehicle electronics and traffic-solutions company, and worked as a design engineer for Interpoint Corporation.



Multichannel DDS Enables Phase-Coherent FSK Modulation

By David Brandon

Common single-channel direct-digital synthesizers (DDS) produce phase-continuous frequency transitions, as shown in Figure 1. In applications such as coherent pulse Doppler radar and NMR/MRI spectrometry for medical and material analysis, however, phase-coherent transitions are preferred. This article demonstrates how to configure the AD9958/AD9959 multichannel DDS as a robust phase-coherent frequency-shift keyed (FSK) modulator by summing the DDS outputs.

A multichannel DDS virtually eliminates channel-to-channel temperature and timing issues encountered when synchronizing multiple single-channel devices. Multichannel DDS outputs, though independent, share the same system clock, allowing them to track better over temperature and power-supply deviations than the outputs of multiple single-channel devices. As a result, a multichannel DDS is better suited for producing phase-coherent frequency transitions at the summed output.

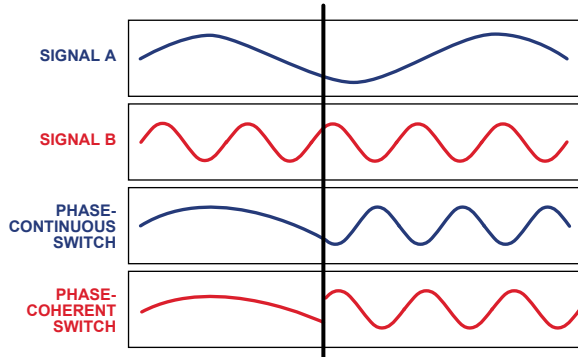


Figure 1. Phase-continuous and phase-coherent frequency transitions.

Circuit Description

The AD9520 clock distribution device drives the AD9958 DDS with a high-performance reference clock, while providing the same clock to the source for the FSK data stream. The AD9520 provides multiple output logic choices and adjustable delays to meet setup- and hold times between the FSK data stream and SYNC_CLK of the multichannel DDS.

The AD9958's two independent channels operate at preprogrammed frequencies F1 and F2. Wiring the outputs together sums them. The profile pins, which drive the multiplier at each DAC input to control the output amplitude, switch the channel outputs on or off to select the desired frequency. To accomplish this, each multiplier has two preprogrammed profile-selectable settings, zero- and

full scale. Logic low on the profile pins shuts off the sine wave while logic high passes it to the output. The operation requires two complementary input data streams to alternate between frequencies. Note that the two DDS channels continuously generate F1 and F2. The off feature mutes the appropriate DDS output, thereby producing a phase-coherent FSK signal.

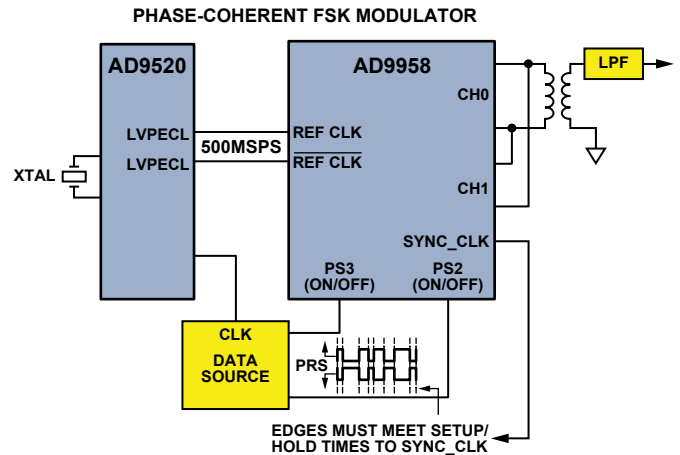


Figure 2. Setup for phase-coherent FSK modulator.

The AD9959 4-channel DDS produced the results shown in Figure 3. Its two additional channels serve as a phase reference for the two switched frequencies at the summed output, making it easier to demonstrate the phase-coherent switching. The summed output, shown in the upper trace, exhibits phase-coherent switching. The middle two traces show reference signals F1 and F2. The bottom trace shows the pseudo-random sequence (PRS) data stream that selects between the two frequencies. Note the edges of the PRS data stream do not align exactly with the frequency transitions of the summed outputs due to the pipeline delay within the device.

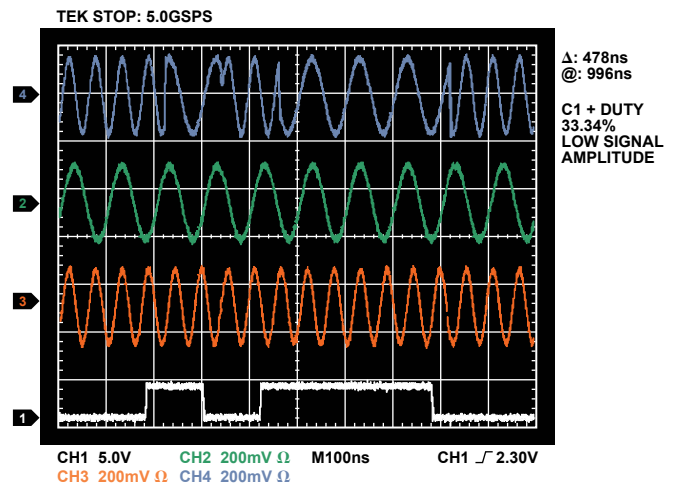


Figure 3. Measured phase-coherent FSK transition.

Figure 4 shows an example of phase-continuous FSK switching, also produced by the AD9959. This type of operation requires less bandwidth, but does not maintain phase memory between transitions.

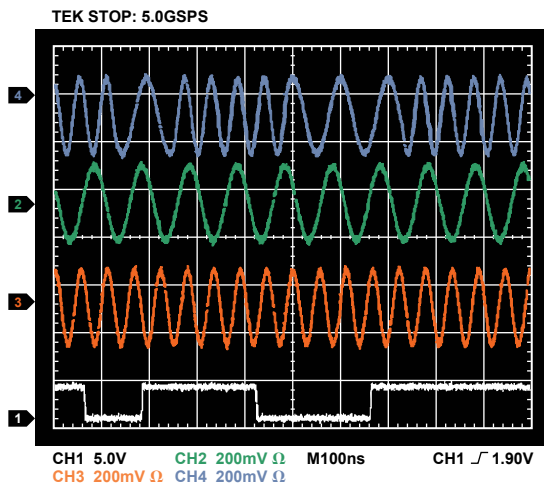


Figure 4. Measured phase-continuous FSK transition.

Analog Devices offers a variety of direct digital synthesizers, clock distribution chips, and clock buffers to build a DDS-based clock generator. Refer to www.analog.com/dds and www.analog.com/clock for more information.

Multichannel, 10-Bit, 500-MSPS Direct Digital Synthesizers

The 2-channel AD9958 (Figure 5) and 4-channel AD9959 direct digital synthesizers (DDS) include two/four 10-bit, 500-MSPS current-output DACs. All channels share a common system clock, providing inherent synchronization; interconnecting multiple devices enables higher channel counts. Independent control of each channel's frequency, phase, and amplitude allows the devices to correct for system-related mismatches. All parameters can be swept linearly; or 16 levels can be chosen for FSK, PSK, or ASK modulation. Output sine wave tuning has 32-bit frequency resolution, 14-bit phase resolution, and 10-bit amplitude resolution. Operating with a 1.8-V core supply, plus a 3.3-V I/O supply for logic compatibility, the AD9958/AD9959 consume 315 mW/540 mW with all channels on, and 13 mW in power-down mode. Specified from -40°C to $+85^{\circ}\text{C}$, they are available in 56-lead LFCSP packages and priced at \$20.48/\$37.59 in 1000s.

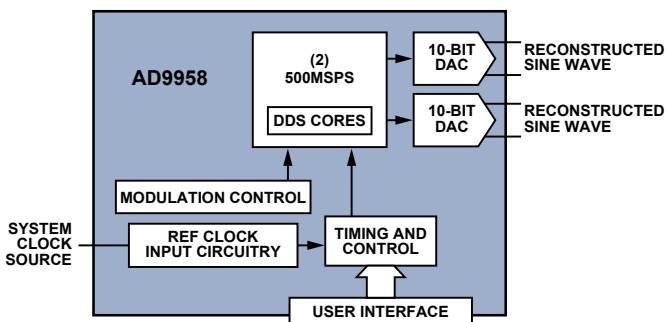


Figure 5. AD9958 functional block diagram.

Clock Generator Has 12 LVPECL/24 CMOS Outputs

The AD9520-x clock generator (Figure 6) derives up to 12 LVPECL or 24 CMOS clocks from a single reference frequency. Integrating a complete PLL with VCO, programmable dividers,

and configurable output buffers, it performs with subpicosecond jitter. Four options provide an on-chip VCO with center frequencies ranging from 1.45 GHz to 2.95 GHz; a fifth option operates with an external VCO at frequencies up to 2.4 GHz. Accepting one differential- or two single-ended references, at frequencies up to 250 MHz, the devices provide four groups of three LVPECL clocks at frequencies up to 1.6 GHz. Programmable dividers, with a divide ratio of 1 to 32, set the output frequency and the coarse delay for each group. Each LVPECL output can be reconfigured to provide two 250-MHz CMOS outputs. Operating on a single 3.3-V supply, the AD9520-x consume 1.5 W max; separate output-driver and charge-pump supplies can be used for logic compatibility and to support VCOs having an extended tuning range. Available in 64-lead LFCSP packages, they are specified from -40°C to $+85^{\circ}\text{C}$ and priced at \$12.65 in 1000s.

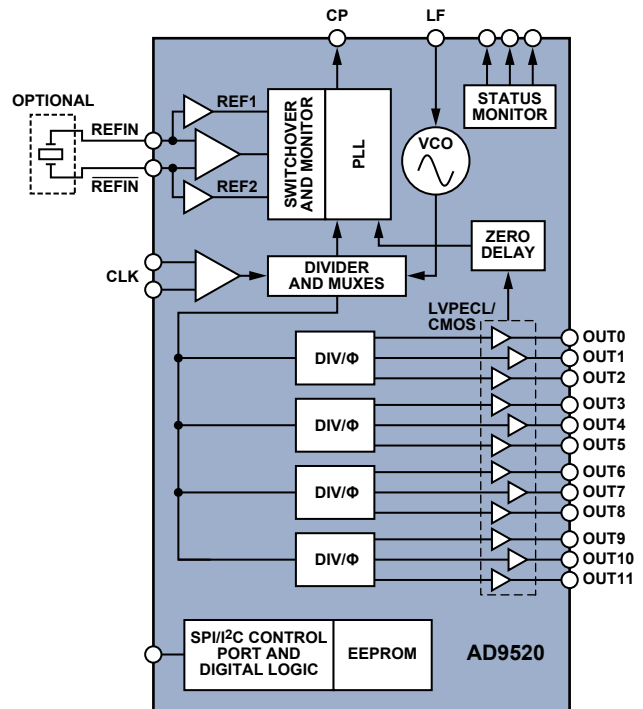


Figure 6. AD9520 functional block diagram.

Further Reading

1. AN-837 Application Note, *DDS-Based Clock Jitter Performance vs. DAC Reconstruction Filter Performance*.
2. Kester, Walt. *The Data Conversion Handbook*. Analog Devices. Chapters 6 and 7. 2005.
3. Kester, Walt. *High Speed System Applications*. Analog Devices. Chapters 2 and 3. 2006.
4. MT-101 Tutorial, *Decoupling Techniques*.
5. MT-031 Tutorial, *Grounding Data Converters and Solving the Mystery of AGND and DGND*.

Author

David Brandon [david.brandon@analog.com] has supported DDS products since the first DDS released back in 1995. His career spans 28 years at ADI, with the last 11 years as an applications engineer in the Clock and Signal Synthesis Group. He has authored a number of application notes and a couple of magazine articles.



High-Side Current Sensing with Wide Dynamic Range: Three Solutions

By Neil Zhao, Wenshuai Liao, and Henri Sino

Introduction

Current sensing is a critical function, necessary for precision closed-loop control in applications such as motor control, solenoid control, communications infrastructure, and power management. End uses range from safety-critical automotive and industrial applications to handheld devices, where power and efficiency are essential. Precision current monitoring allows designers to obtain critical instantaneous information, such as motor torque—based on motor current—efficiency of a dc-to-dc converter, or bias current in a base station’s LDMOS (laterally diffused MOS) power transistor, or diagnostic information, such as shorts to ground.

To understand the key trade-offs, options, and challenges faced by system designers when choosing the most accurate, cost-effective current sensor for a circuit board, we take a close look at current sensing in LDMOS bias current monitoring in cellular base station power amplifiers and other relevant applications.

Current monitoring is necessary in base station power amplifiers, especially with the more complex modulation methods used in 3G and LTE, where the peak-to-average power ratio varies from 3.5 dB (about 2.2 to 1) for 3G W-CDMA to 8.5 dB (about 7.1 to 1) for LTE OFDM—compared with 3 dB (about 2 to 1) for the most popular 2G single-carrier GSM. One of the control-loop functions is to monitor the LDMOS bias current, which allows the bias of the LDMOS to be properly modulated for a given power output. Typically, this dc bias current has a wide dynamic range based on operating, maximum, or off-peak operation. To the designer, this means that an accurate current sensor is needed to monitor a current that can range from 50 mA (or as little as 15 mA)¹ to 20 A, while the drain of the LDMOS is biased at a high voltage ranging from 28 V to 60 V. Using a shunt resistor to monitor this current means that the designer is limited to a very small shunt that will not dissipate too much power when the LDMOS current is 20 A. As an example, even a 10 mΩ shunt will dissipate 4 W at maximum current.

While shunt resistors are available to handle this power, lower power dissipation might be a requirement of the board. But the choice of such low resistance values means that at low currents, say 50 mA, the voltage across the 10 mΩ shunt is extremely small (500 μV), making it a challenge to monitor accurately—with a circuit that must also withstand high common-mode voltage.

This article will focus on providing current-sensing solutions that can help designers accurately monitor wide-ranging dc currents in the presence of high common-mode voltages. Special attention will also be devoted to temperature performance, a critical parameter that is often not easy to calibrate but must be faced in the case of outdoor power amplifiers. Three optional solution approaches are described here—in order of decreasing design complexity—that provide viable high-accuracy, high-resolution current sensing for a variety of applications.

1. Use discrete components, such as op amps, resistors, and Zener diodes, to build a current sensor. This solution employs the AD8628 zero-drift amplifier as its key component.

2. Attain an increased level of integration by using a high voltage bidirectional current shunt monitor, such as the AD8210, with additional external components to extend dynamic range and accuracy.
3. Employ an application-optimized device such as the newly available AD8217, an easy-to-use, highly integrated zero-drift current sensor with an input common-mode voltage range of 4.5 V to 80 V.

Configuring a Standard Op Amp for High-Side Current Sensing

Figure 1 shows an op-amp-based discrete solution employing the AD8628. The same setup is valid with other op amps as well, but specific features that are required include low input offset voltage, low offset voltage drift, low input bias current, and rail-to-rail input- and output swing capability, if possible. Other recommended amplifiers include the AD8538, AD8571, and AD8551.

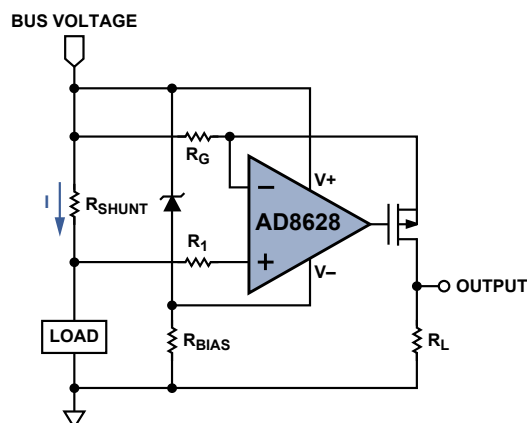


Figure 1. Discrete high-current sensing solution using an operational amplifier.

This circuit monitors the high-side current, I . The amplifier is biased *on* via the Zener diode, which, in this case, is rated at 5.1 V. Its use ensures that the amplifier operates safely at the high common-mode level and that its supply voltage remains steady and within the allowed supply limits, while the output is converted to a current by the MOSFET—and to a ground-referenced voltage by resistor R_L . The output voltage can thus feed converters, analog processors, and other ground-referenced components—such as op amps or comparators—for further signal conditioning.

In this configuration, the voltage across R_G is equal to the voltage across R_{SHUNT} because feedback via the MOSFET maintains both high-impedance op-amp inputs at the same voltage. The current through R_G flows through the FET and R_L to develop V_{OUTPUT} . The relationship between the current, I , flowing through the shunt resistor and V_{OUTPUT} is expressed by Equation 1:

$$V_{OUTPUT} = \frac{I \times R_{SHUNT}}{R_G} \times R_L \quad (1)$$

R_{SHUNT} Selection: The maximum value of R_{SHUNT} is limited by the allowable power consumption at maximum current. The minimum value of R_{SHUNT} is limited by the input range and error budget of the op amp. Normally, the value of R_{SHUNT} is from 1 mΩ to 10 mΩ for monitoring currents greater than 10 A. If a single resistor cannot meet the power consumption requirement or is too large for the PCB, R_{SHUNT} may have to be made up of multiple resistors in parallel.

¹According to Antenna Interface Standards Group (AISG) 1.1.

R_G Selection: R_G is used to translate a current proportional to the high-side current to the low-side. The maximum R_G is limited by the drain-source leakage current of the P-channel MOSFET. For example, consider the common P-channel enhancement-mode vertical DMOS transistor BSS84. The maximum I_{DSS} at various conditions is shown in Table 1.

Table 1. Drain-Source Leakage Current

Conditions	Maximum I_{DSS}
$V_{GS} = 0\text{ V}; V_{DS} = -40\text{ V}; T_j = 25^\circ\text{C}$	-100 nA
$V_{GS} = 0\text{ V}; V_{DS} = -50\text{ V}; T_j = 25^\circ\text{C}$	-10 μA
$V_{GS} = 0\text{ V}; V_{DS} = -50\text{ V}; T_j = 125^\circ\text{C}$	-60 μA

Consider the LDMOS drain current monitoring example, with 28-V common mode and I_{DSS} of 100 nA. The mirror of the minimum current through R_L should be at least 20 times I_{DSS} . This results in

$$R_{G_MAX} = \frac{I_{MIN} \times R_{SHUNT}}{20 \times 100\text{ nA}}$$

The minimum R_G is limited by allowable mirror current power consumption at maximum load current

$$R_{G_MIN} = \frac{I_{MAX} \times R_{SHUNT}}{I_{MIRROR_MAX}}$$

R_{BIAS} Selection: The current through R_{BIAS} divides to produce the op amp's quiescent current and the essentially constant Zener-diode voltage, V_Z , (which determines the op amp's supply voltage). Make sure the current flowing through the Zener diode does not exceed its maximum regulated current, I_{Z_MAX} , when the amplifier current, I_{SUPPLY} , is essentially zero and V_{IN} is the maximum:

$$R_{BIAS_MIN} = \frac{V_{IN_MAX} - V_Z}{I_{Z_MAX}}$$

To ensure a stable diode voltage, the current flowing through it should be higher than its minimum operating current, I_{Z_MIN} , when I_{SUPPLY} is the maximum and V_{IN} is the minimum:

$$R_{BIAS_MAX} = \frac{V_{IN_MIN} - V_Z}{I_{Z_MIN} + I_{SUPPLY_MAX}}$$

The Zener diode and R_{BIAS} are the key components in this solution because they take away the high common-mode voltage from the following circuits and allow the use of a low-voltage precision op amp. For best voltage stability, the Zener diode should have low dynamic resistance and low temperature drift.

R_1 Selection: R_1 is used to limit the amplifier input current if input transients exceed the op amp's power supply voltage. A 10-k Ω resistor is recommended.

The offset voltage, V_{OS} , and offset current, I_{OS} , of the chosen op amp are critical, especially with low values of shunt resistance and at low load currents. $V_{OS} + I_{OS} \times R_1$ must be smaller than $I_{MIN} \times R_{SHUNT}$, or the amplifier may be saturated. Therefore, a rail-to-rail input amplifier with zero crossover distortion is preferred for optimal performance.

Another issue to consider for this discrete solution is temperature drift. Even if an amplifier with zero drift is used, it is very difficult or costly to optimize drifts caused by discrete components: the Zener diode, MOSFET, and resistors. From Table 1, the maximum I_{DSS} of the MOSFET changes from -10 μA to -60 μA as the operating temperature changes from 25 $^\circ\text{C}$ to 125 $^\circ\text{C}$ with $V_{GS} = 0\text{ V}$ and $V_{DS} = -50\text{ V}$. This drift will degrade the system

accuracy over temperature, especially when the monitored current is low. The drift of the Zener diode will impact the stability of the amplifier's power supply, so the amplifier used should have high power-supply rejection (PSR).

Further, designers must take into account the low power efficiency of this solution: A lot of power is consumed by R_{BIAS} . For example, if the bus common-mode voltage is 28 V, the Zener-diode voltage output is 5.1 V, and R_{BIAS} is a 1000- Ω resistor, the circuit will dissipate more than 0.52 W of undesirable power. This adds to the power-consumption budget and must be taken into account.

High-Side Current Sensing with the AD8210 and External Components

Figure 2a shows a simplified block diagram of the AD8210 integrated high-voltage bidirectional current shunt monitor; Figure 2b shows a unidirectional application with an external voltage reference.

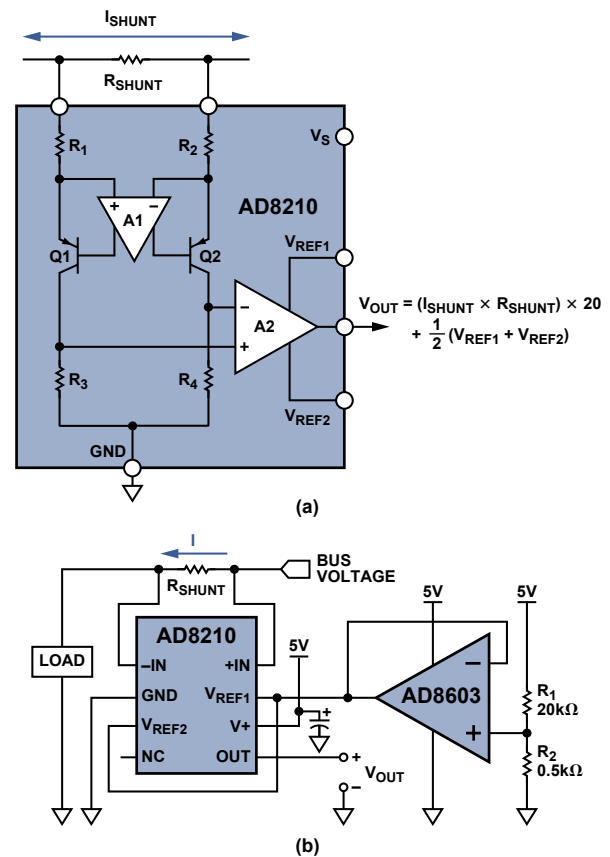


Figure 2. (a) AD8210 high-voltage bidirectional current shunt monitor. (b) Wide-range unidirectional application with an external reference.

The AD8210 amplifies a small differential input voltage generated by a positive or negative current flowing through the shunt resistor. The AD8210 rejects high common-mode voltages (up to 65 V) and provides a ground-referenced buffered output.

As shown in Figure 2a, it comprises two main blocks, a differential amplifier, and an instrumentation amplifier. The input terminals are connected to differential amplifier A1 via R_1 and R_2 . A1 nulls the voltage appearing across its own input terminals by adjusting the small currents through R_1 and R_2 with Q1 and Q2. When the input signal to the AD8210 is 0 V, the currents in R_1 and R_2 are equal. When the differential signal is nonzero, the current increases through one of the resistors and decreases in the other. The current difference is proportional to the size and polarity of the input signal.

The differential currents through Q1 and Q2 are converted into a differential voltage by R_3 and R_4 . A2 is configured as an instrumentation amplifier. The differential voltage is converted into a single-ended output voltage by A2. The gain is internally set to 20 V/V with precision-trimmed, thin film resistors.

The output reference voltage is easily adjusted using the V_{REF1} and V_{REF2} pins. In a typical configuration for handling bidirectional current flow, V_{REF1} is connected to V_{CC} while V_{REF2} is connected to GND. In this case, the output is centered at $V_{CC}/2$ when the input signal is 0 V, so with a 5-V supply the output is centered at 2.5 V. The output will be greater or less than 2.5 V, depending on the direction of the current through the shunt resistor.

This configuration works well for charge/discharge applications, but if the user needs to utilize the entire output range to measure a unidirectional current flow, then the circuit of Figure 2b shows a typical way that an external source may be used to set the range. Here a resistive divider is buffered by an op amp to drive the V_{REF1} and V_{REF2} pins, connected together, to offset the output.

It is difficult for the amplifier alone to monitor the load current as it comes close to zero. With a 5-V supply, the AD8210 specifies a linear output range with a minimum output of 50 mV and a maximum output of 4.9 V. Consider an application where the shunt resistance is 10 m Ω . The minimum current through it must be greater than 250 mA to ensure that the output of the AD8210 is above its lowest point of 50 mV.

$$V_{OUT} = I_{SHUNT} \times R_{SHUNT} \times Gain \\ = 250 \text{ mA} \times 10 \text{ m}\Omega \times 20 = 50 \text{ mV}$$

The configuration shown in Figure 2b adds an offset to allow smaller currents to be measured. The relationship between output voltage and monitor current, based on an amplifier gain of 20 V/V, can be calculated as Equation 2:

$$V_{OUTPUT} = I \times R_{SHUNT} \times Gain \text{ of AD8210} \\ + \left[5 \text{ V} \times \frac{R_2}{R_1 + R_2} \right] \quad (2)$$

For example, using resistances, R_1 and R_2 , of 9800 Ω and 200 Ω , respectively, the offset voltage will be 100 mV. When the differential input is 0 V, the AD8210 output will now be 100 mV, safely in the linear range. If the range of shunt current is from 50 mA to 20 A, with $R_{SHUNT} = 10 \text{ m}\Omega$, the input range would be 0.5 mV to 200 mV; and the output range of the AD8210 is 10 mV to 4 V plus the offset voltage, or 0.11 V to 4.1 V, well within the AD8210's specified linear range.

In fact, using this configuration, the designer can offset the output of the AD8210 to any point within its supply range in order to handle arbitrary current ranges having any degree of asymmetry. An op amp to buffer the voltage divider is desirable because precision-trimmed resistances are connected internally to the reference inputs—so, for best results, those inputs should be driven at low impedance. Precision and low cost op amps that can be used to buffer the external reference include—for example—the AD8541, AD8601, AD8603, AD8605, AD8613, AD8691, and AD8655.

Compared with the discrete solution, this integrated solution requires that the current shunt monitor have high common-mode voltage range and an output offset—if the output voltage range cannot meet the current-detection range requirements. But it can handle bidirectional current monitoring, and it avoids the temperature drift and power consumption issues described above. The offset drift and gain drift of the AD8210 are guaranteed to be

a maximum of 8 $\mu\text{V}/^\circ\text{C}$ and 20 ppm/ $^\circ\text{C}$, respectively. And if, for example, the AD8603 were used as the buffer, it would contribute an offset of only 1 $\mu\text{V}/^\circ\text{C}$, which can be neglected compared with the AD8210's already low offset-voltage drift. The power consumption of the divider, R_1 and R_2 , is

$$\frac{(5 \text{ V})^2}{R_1 + R_2}$$

or only 1.2 mW, using the parameters in Figure 2b.

High-Side Current Monitoring Using the Zero-Drift AD8217

Recently, Analog Devices introduced the AD8217, a high-voltage current sensor featuring zero drift and 500-kHz bandwidth, designed specifically to enhance resolution and accuracy over wide temperature-, input common-mode-, and differential voltage ranges. Figure 3a shows a simplified block diagram of the device; Figure 3b shows it in a typical application.

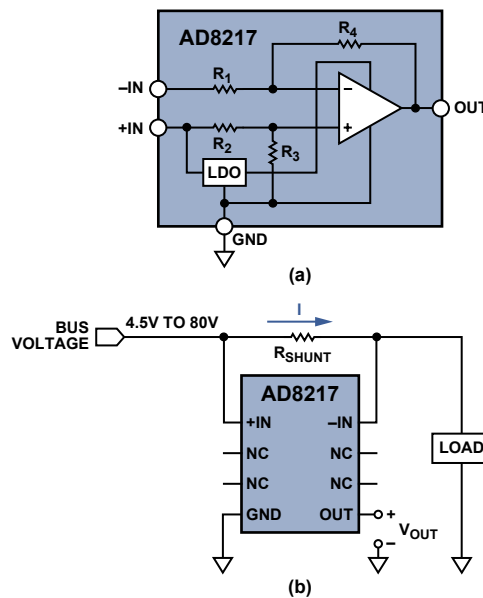


Figure 3. (a) The AD8217 high-resolution, zero-drift current-shunt monitor. (b) High-side current sensing using the AD8217.

For measuring very small currents through a small shunt resistor, the AD8217 features a minimum 20-mV output range over temperature, an improvement over the AD8210's 50-mV range. Thus, if the minimum load current being monitored across the shunt produces 20-mV minimum output, which is 1-mV minimum input, from the current sensor, then the user can choose the AD8217 configured as shown in Figure 3b. The relationship between the output voltage of the AD8217 and the input current can be calculated as Equation 3:

$$V_{OUTPUT} = I \times R_{SHUNT} \times 20 \quad (3)$$

The AD8217 features an internal *low-dropout regulator* (LDO), which provides a constant-voltage supply to the amplifier. The LDO withstands the high common-mode voltage that can vary from 4.5 V to 80 V, essentially performing a similar function to that of the Zener diode in Figure 1.

The AD8217 features a factory-set gain of 20 V/V, with a maximum $\pm 0.35\%$ gain error over the entire temperature range. The initial offset, specified $\pm 300 \mu\text{V}$ over temperature, and the miniscule temperature drift, $\pm 100 \text{ nV}/^\circ\text{C}$, will enhance any error budget. The buffered output voltage directly interfaces with any typical analog-to-digital converter. Regardless of the common mode,

the AD8217 provides the correct output voltage when the input differential is at least 1 mV. Using a 10-mΩ shunt resistor, as above, the minimum current can be as low as 100 μA.

The single-chip solution avoids the temperature drift and power consumption issues of the discrete solution.

Performance Results Compared

The following section will display test results obtained comparing the three different methods. The input current through the shunt was adjusted by changing both the input voltage and load resistance. In the data, initial calibration has been performed in order to remove the initial gain and offset errors associated with all the parts used in our board.

Figure 4 is a linearity plot of the output voltage across R_L as a function of low-end values of input current flowing through R_{SHUNT} , measured using the circuit of Figure 1. R_{SHUNT} is 10 mΩ; R_G is 13 Ω; R_{BIAS} is 100 Ω; R_1 is 10 kΩ; load resistance is 200 Ω; R_L is 200 Ω; the Zener diode output is 5.1 V; the op amp is AD8628; the MOSFET is BSS84. The maximum relative error is 0.69%, and the average is 0.21% after calibration.

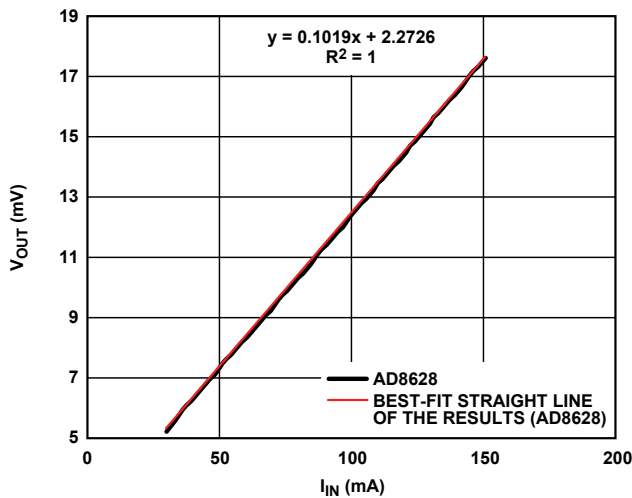


Figure 4. Low-current test result with AD8628 in Figure 1.

Figure 5 is a linearity plot of the output voltage of the AD8210 as a function of low-end values of input current flowing through R_{SHUNT} , measured using the circuit of Figure 2b. R_{SHUNT} is 10 mΩ; R_1 is 20 kΩ; R_2 is 0.5 kΩ; the load resistance is 200 Ω. The external reference buffer is an AD8603. The maximum relative error is 0.03%, and the average is 0.01% after calibration.

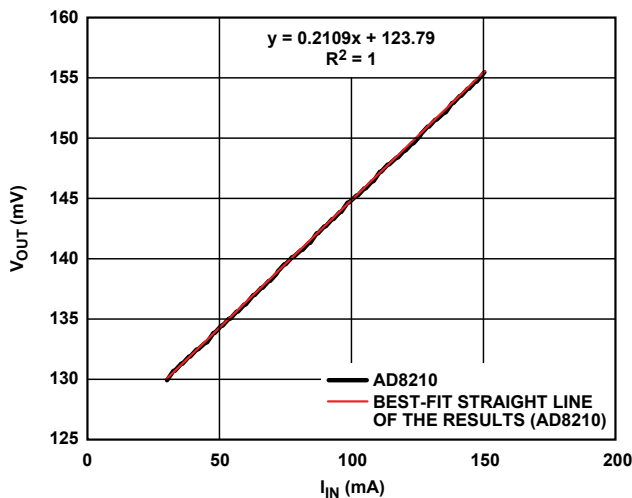


Figure 5. Low-current test result with AD8210 in Figure 2b.

Figure 6 is a linearity plot of the output voltage of the AD8217 vs. low-end values of input current flowing through R_{SHUNT} in the circuit of Figure 3b. R_{SHUNT} is 10 mΩ, and the load resistance is 50 Ω. The maximum relative error is 0.088%, and the average is 0.025% after linear correction.

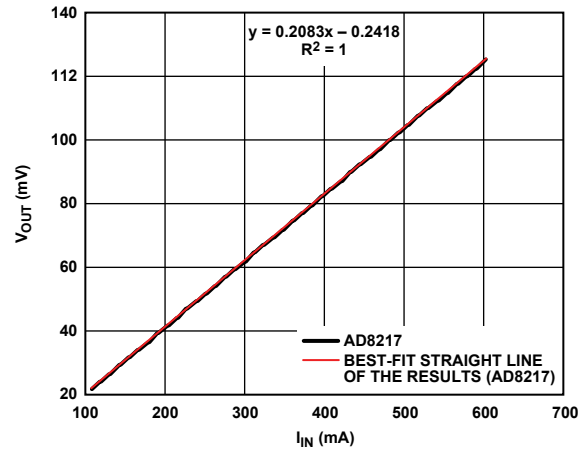


Figure 6. Low-current test result with AD8217 in Figure 3b.

Note that the tests were necessarily concentrated at the low end of the range and did not cover the full 50 μA to 20 A range. The reason is that the linearity challenge is mainly at the low output voltage (low unipolar current) portion of the range.

Temperature experiments were also done for each solution at -40°C , $+25^{\circ}\text{C}$, and $+85^{\circ}\text{C}$. Table 2 shows the maximum relative error and average error when using the same correction factor at $+25^{\circ}\text{C}$ to calibrate the data at -40°C and $+85^{\circ}\text{C}$.

Table 2. Maximum and Average Error at Different Temperatures Using the Same Correction Factor

Solution Circuit		AD8628	AD8210	AD8217
-40°C	Max error (%)	11.982	2.117	0.271
	Avg error (%)	4.929	2.059	0.171
$+25^{\circ}\text{C}$	Max error (%)	1.806	0.075	0.103
	Avg error (%)	0.228	0.039	0.022
$+85^{\circ}\text{C}$	Max error (%)	6.632	3.800	0.918
	Avg error (%)	5.769	3.498	0.421

If a temperature sensor is available for use in the system, different correction factors can be used to calibrate the data at different temperatures, but with increased component and manufacturing cost. Table 3 shows the maximum relative error and average error when different correction factors are used at -40°C , $+25^{\circ}\text{C}$, and $+85^{\circ}\text{C}$.

Table 3. Maximum and Average Error at Different Temperatures Using Different Correction Factors

Solution Circuit		AD8628	AD8210	AD8217
-40°C	Max error (%)	1.981	0.022	0.114
	Avg error (%)	0.303	0.009	0.023
$+25^{\circ}\text{C}$	Max error (%)	1.806	0.075	0.103
	Avg error (%)	0.228	0.039	0.022
$+85^{\circ}\text{C}$	Max error (%)	1.844	0.038	0.075
	Avg error (%)	0.241	0.013	0.020

The temperature experiments show the high accuracy available over wide temperature ranges with devices using auto-zero technology, especially in the case of the AD8217.

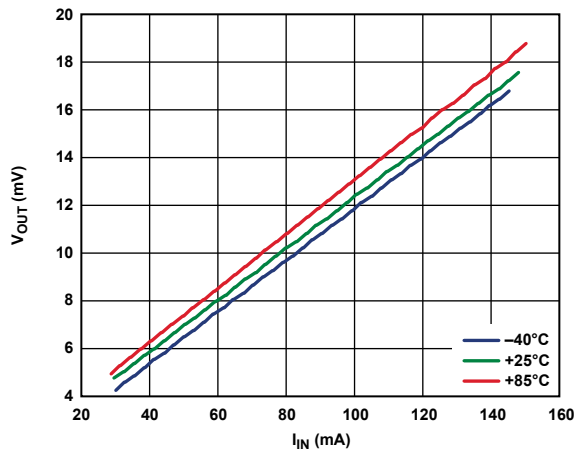


Figure 7. Temperature experiment using discrete solution with AD8628.

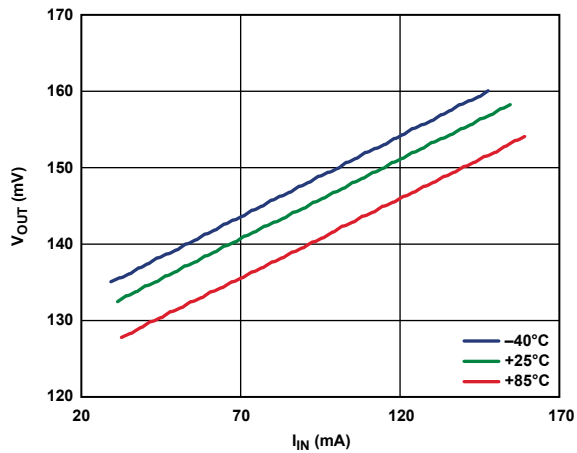


Figure 8. Temperature experiment using integrated solution with AD8210.

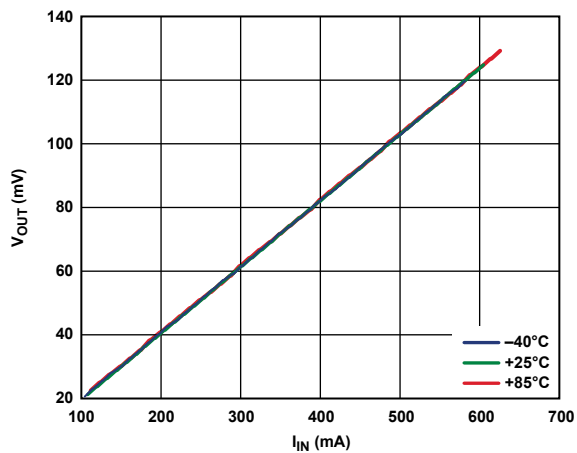


Figure 9. Temperature experiment using single-chip solution with AD8217.

Conclusion

The test results show that all three solutions can be used for wide dynamic range high-side current sensing: the outputs are linear in all three solutions, while the solution using the AD8217 leads to the best error performance without the necessity of a standalone power supply. The $\pm 100\text{-nV}/^\circ\text{C}$ offset drift characteristic also makes it ideal for the most accurate performance throughout the -40°C to $+125^\circ\text{C}$ temperature range. From a system design perspective, the single-chip solution can save PCB area, ease PCB layout, decrease system cost, and improve reliability. These findings apply particularly to unidirectional current sensing applications, where the load-current range is wide and dynamic range is critical.

Based on these test results, the AD8217 solution is the most suitable of the three choices for wide dynamic range unidirectional high-side current sensing and monitoring. We also note that an AD8210 solution offers operation right down to 0-V inputs—which could be beneficial for short-to-ground conditions. Note also that the AD8210 is capable of single-chip monitoring of bipolar current flow, as in charge/discharge applications.

Calibration and temperature sensing are recommended in practical system designs requiring best system performance.

Acknowledgment

Mr. Ryan Du contributed to the discrete solution setup and measurement portion of this article while interning at Analog Devices.

Authors

Neil Zhao (neil.zhao@analog.com) is an applications engineer in ADI's Micromachined Products Division in Beijing, China. Previously, he was a field applications engineer in ADI's China Applications Support Team, where he had been working for nearly three years. Neil graduated in January 2008 from Beihang University with a master's degree in communication and information systems.



Wenshuai Liao (wenshuai.liao@analog.com) is a marketing engineer in ADI's Integrated Amplifier Products (IAP) Group in Beijing, China. After earning a master's degree in optical engineering from Tsinghua University, Wenshuai spent three years as a TD-SCDMA Node B RF engineer at Datang Telecommunications Group. He joined ADI in 2002.



Henri Sino (henri.sino@analog.com) is an applications engineer in the Integrated Amplifier Products (IAP) Group at Analog Devices in Wilmington, MA. Henri has been with ADI for six years, since obtaining a BSEE from Worcester Polytechnic Institute. During his time at ADI, Henri has mainly focused on supporting products and customers relating to the automotive and communications markets.



Boost Supply and High-Voltage DAC Provide Tuning Signal for Antennas and Filters

By Ken Kavanagh

Antenna arrays and filters are often tuned by varying the voltage on a barium strontium titanate (BST) capacitor. When this ferroelectric material is used in capacitors, an applied voltage causes a small variation in the crystal structure, which changes the dielectric constant and, therefore, the capacitance. Electronically tunable BST capacitors can handle higher power and larger signal amplitude than the conventional varactor diodes.

In typical applications, the tuning capacitor compensates for component tolerance, adjusts the cutoff frequency of a filter, or matches the network impedance of a tunable antenna. The BST capacitor is tuned by applying a voltage between 0 V and 30 V. As power supplies in modern electronic devices trend toward lower voltages, 3.3-V, 2.5-V, or even 1.8-V supplies are common, especially in battery-powered applications. Despite the benefits of tuning, it does not always make sense to add a separate high-voltage supply for this function alone. Thus, a convenient way to generate the power supply is required.

In this application, for example, a 3-V power supply is available, but the BST capacitors require voltages in excess of 20 V for full control. The two main circuit blocks are the ADP1613 step-up switching converter and the AD5504 high-voltage DAC. The circuit shown in Figure 1 generates DAC output voltages up to 30 V. The DAC outputs set the bias voltages for the BST capacitors, thus adjusting the antenna response.

The AD1613 step-up dc-to-dc switching converter (Figure 4) integrates a power switch capable of providing an output as high as 20 V. Higher voltages can be achieved by using external components. As shown, the ADP1613 generates a 32-V output from a 3-V input. The ADIsimPower™ tool¹ provides an easy way for designers to determine the appropriate components based on the input requirements.

The 32-V output from the ADP1613 powers the AD5504 quad, 12-bit, high-voltage DAC (Figure 5), which can provide up to 60 V on each of its four outputs. The voltage on the $\overline{R_SEL}$ pin determines its full-scale output. In this application, $\overline{R_SEL}$ is connected to V_{DD} , setting the full-scale output to 30 V. The DAC registers are updated via the 3-V compatible serial interface. All four DACs are updated simultaneously by pulsing the load pin (\overline{LDAC}) low, thus allowing four BST capacitances to be changed at the same time.

Figure 2 shows the equivalent circuit of a BST capacitor used as a tunable matching network. Figure 3 shows the transfer function of the BST capacitance vs. voltage and the antenna response. BST capacitors can be obtained from suppliers such as Agile RF.²

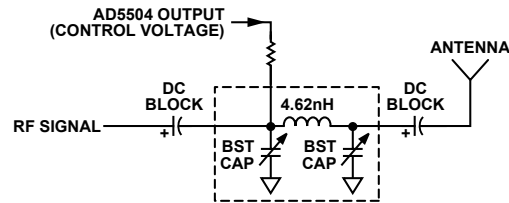


Figure 2. BST capacitor equivalent circuit.

Circuits such as that of Figure 1 can benefit next-generation mobile phones, which are being pressured by two opposing forces. On one side is the ever-present requirement to reduce size and power consumption. On the other is the need to increase performance, utilizing more frequency bands by inserting more antennas and radio systems into a smaller volume. Antenna designers are reaching physical design limits with regard to volume and efficiency, as decreasing antenna volume decreases efficiency. Tunable antennas solve this problem in multiband, multimode phones and can extend the operating frequency range of a cell phone, switching from US GSM850 to European GSM900, for example, while maintaining size and efficiency. In multiuse devices, different head and hand positions used while texting, talking, or surfing the Web present the antenna with different load impedances, detuning the antenna and decreasing signal quality. A tunable impedance matching network can adapt for these varying conditions and recover the detuned signals.

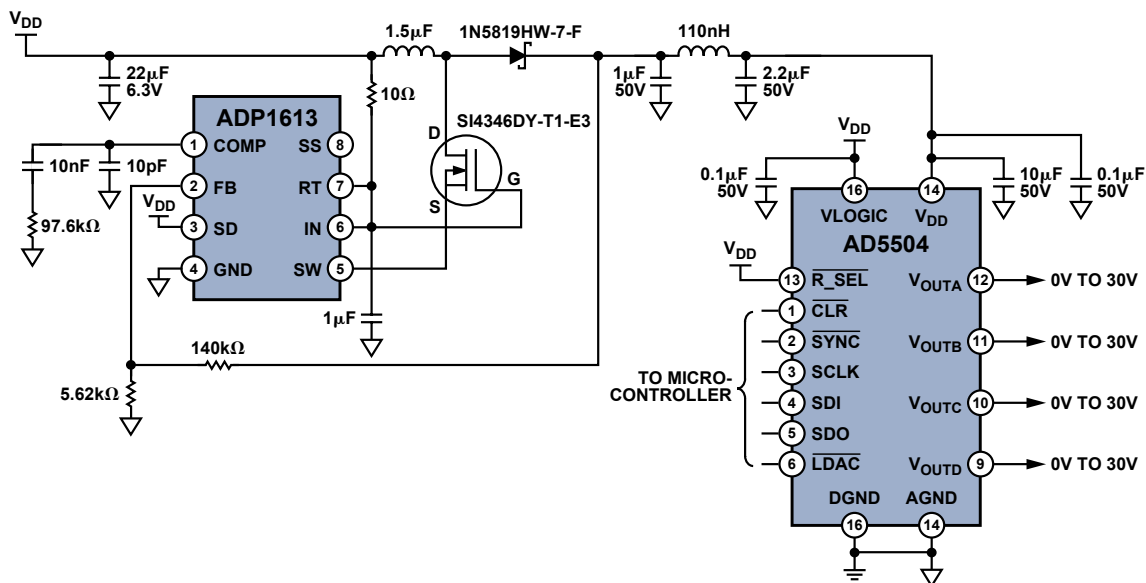


Figure 1. Boost supply and high-voltage DAC provide tuning signal for BST capacitors.

Step-Up DC-to-DC Switching Converter Operates at 650 kHz/1300 kHz

The ADP1613 step-up converter is capable of supplying over 150 mA at voltages as high as 20 V, while operating with a single 2.5-V to 5.5-V supply. Integrating a 2-A, 0.13- Ω power switch with a current-mode, pulse-width modulated regulator, its output varies less than 1% with changes in input voltage, load current, and temperature. The operating frequency is pin-selectable and can be optimized for high efficiency or minimum external component size: at 650 kHz it provides 90% efficiency; at 1.3 MHz its circuit implementation occupies the smallest space, making it ideal for space-constrained environments in portable devices and liquid-crystal displays. The adjustable soft-start circuit minimizes inrush currents, ensuring safe, predictable start-up conditions. The ADP1613 consumes 2.2 mA in the switching state, 700 μ A in the nonswitching state, and 10 nA in shutdown mode. Available in an 8-lead MSOP package, it is specified from -40°C to +85°C and priced at \$0.70 in 1000s.

Quad, 12-Bit DACs Provide High-Voltage Outputs

The AD5504 quad, 12-bit, high-voltage DAC has pin-selectable output ranges of 0 V to 30 V and 0 V to 60 V. Functionally complete, it includes a precision voltage reference, temperature sensor, four double-buffered DACs, and four high-voltage amplifiers. Upon power-up, the digital

section is enabled and set to a known state; the analog section remains disabled until a power-up command is issued via the SPI port. The temperature sensor disconnects the analog outputs and sets an alarm flag if the die temperature exceeds 110°C. The AD5504 specifies 1-LSB max differential nonlinearity (DNL) and 3-LSB max integral nonlinearity (INL) in 30 V mode. Operating on 10-V to 62-V and 2.3-V to 5.5-V supplies, it consumes 2 mA in *normal* mode and 30 μ A in *power-down* mode. Available in a 16-lead TSSOP package, it is specified from -40°C to +105°C and priced at \$9.92 in 1000s.

References

(Information on all ADI components can be found at www.analog.com.)

¹www.analog.com/adisimpower.

²www.agilerf.com.

Author

Ken Kavanagh [ken.kavanagh@analog.com] is an applications engineer in ADI's Precision DAC Group. Currently responsible for providing applications support for the *nanoDAC*[®] and *denseDAC*[®] portfolios, Ken has worked in applications since 1994. He earned a BEng from the University of Limerick in 1999.

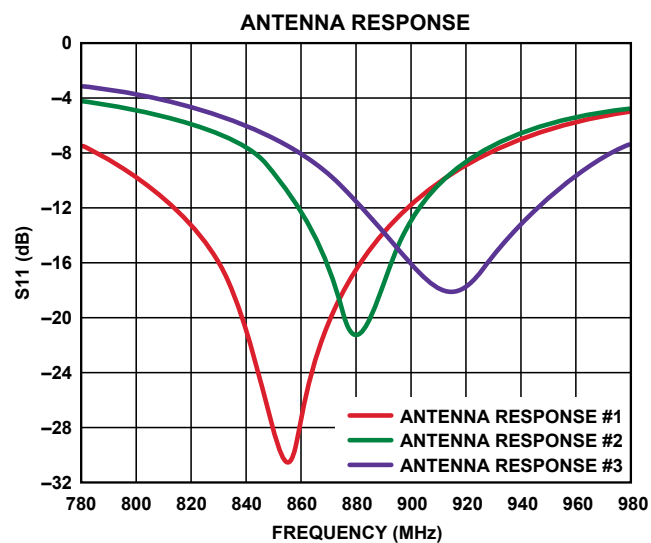
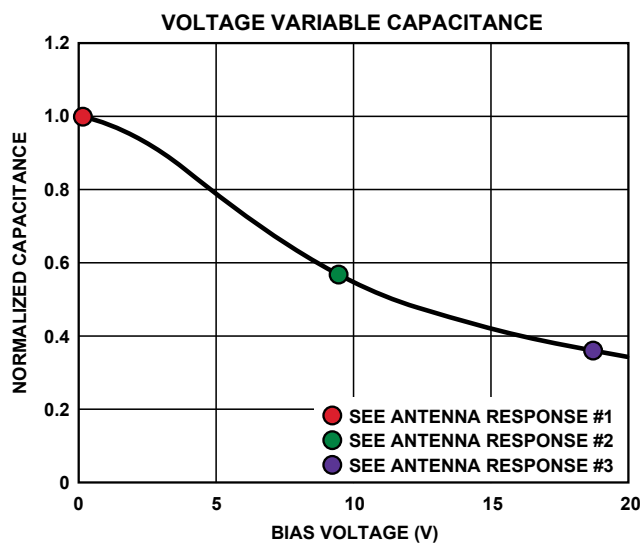


Figure 3. Bias voltage vs. BST capacitance; resulting antenna response.

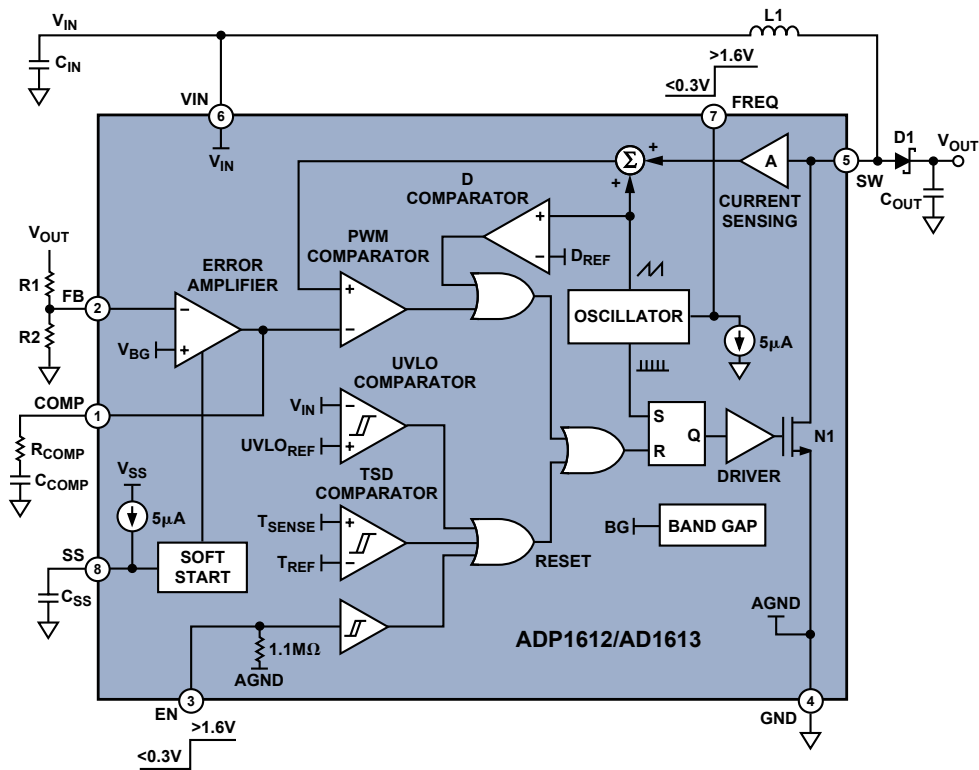


Figure 4. ADP1613 functional block diagram.

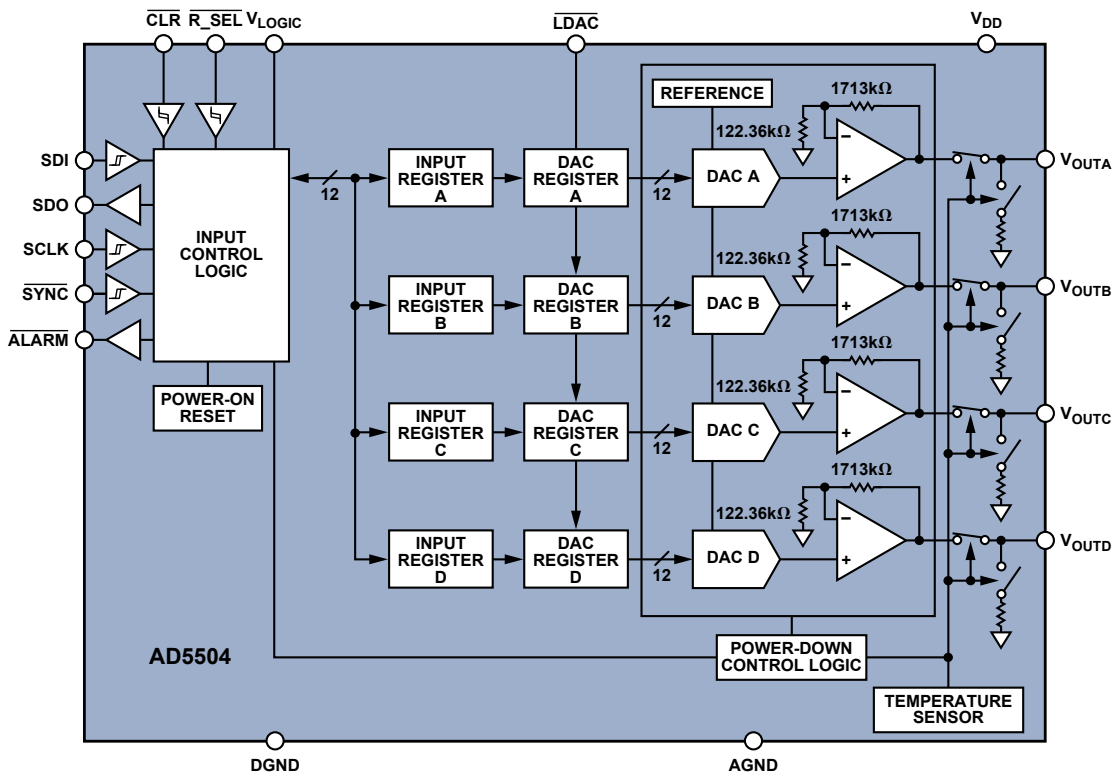


Figure 5. AD5504 functional block diagram.

High-Performance Difference Amplifier with Precision Supply-Referenced Level Shift

By Moshe Gerstenhaber and Michael O'Sullivan

Designed on small-geometry processes, high-performance ADCs typically run on single 1.8-V to 5-V supplies. When processing ± 10 -V or larger signals, an amplifier circuit ahead of the ADC can attenuate the signal to keep it from saturating the ADC inputs. A difference amplifier (diff amp) is commonly used when the signal includes a large common-mode voltage.

The ability of a diff amp to reject a common-mode voltage is determined by the ratio match of the gain-setting resistors; the closer the match, the higher the common-mode rejection (CMR). For discrete amplifiers with 0.1% external resistors, CMR is limited to 54 dB. ICs that integrate precision laser-trimmed resistors with an op amp can achieve CMR better than 80 dB.

Early diff amps, like many other analog ICs, typically operated on dual ± 5 -V to ± 15 -V supplies. As ADCs and other components moved to lower supply voltages, for a time the only circuit requiring dual supplies was the diff amp at the front end. But adding a negative supply for this single circuit was quite inconvenient.

New diff amps can operate on single 2.7-V to 15-V supplies, but the op amp inputs and output would all be pinned to the negative rail (ground) under some operating conditions. To measure signals containing negative common-mode voltages, the common-mode input must be raised off the negative rail. To measure negative signals, the amplifier output must be raised off the negative rail. Both of these level shifts can be accomplished by applying a positive voltage to the *reference* pin. With a single 5-V supply, for example, a 2.5-V source on the reference pin sets the output to midsupply and raises the common-mode voltage seen at the op amp inputs. The source must be low impedance to avoid degrading the CMR and low drift to maintain accuracy over temperature. Figure 1 shows a typical solution that uses two external precision resistors and a low-drift precision op amp.

Figure 2 shows an alternative solution that offers lower cost and higher performance by using the AD8271 difference amplifier, with its multiple integrated precision-trimmed resistors. The on-chip resistors set the device output to midsupply. The resistors are all manufactured from the same low-drift thin-film material, so their ratio match over temperature is excellent; they are trimmed to match the other resistors in the circuit, so they do not degrade the excellent CMR.

Precision Programmable-Gain Difference Amplifier

The AD8271 low-distortion, programmable-gain difference amplifier comprises a precision op amp and seven laser-trimmed gain-setting resistors, enabling user-selectable differential gains of 0.5, 1, or 2. It can also be configured in over 40 single-ended configurations, with gains ranging from -2 to $+3$. Two grades are available: the *B*-grade specifies 0.02% max gain error, 2-ppm/ $^{\circ}$ C max gain drift, 600- μ V max offset, and 80-dB min common-mode rejection; the *A*-grade specifies 0.05% max gain error, 10-ppm/ $^{\circ}$ C

max gain drift, 1000- μ V max offset, and 74-dB min common-mode rejection. Both grades specify -110 -dB harmonic distortion, 15-MHz bandwidth, and 30-V/ μ s slew rate. This combination of speed and precision makes the device ideal for instrumentation amplifiers, driving ADCs, level shifting, and automatic test equipment. Operating on a single 5-V to 36-V supply, or dual ± 2.5 -V to ± 18 -V supplies, the AD8271 draws 2.3 mA. Available in a 10-lead MSOP package, it is specified from -40° C to $+85^{\circ}$ C and priced from \$1.25 in 1000s.

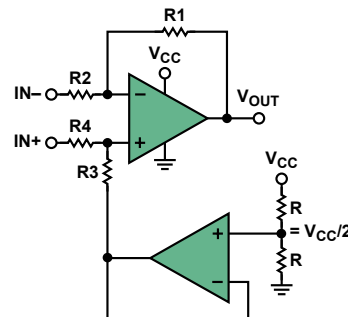


Figure 1. Single-supply difference amplifier with midsupply output.

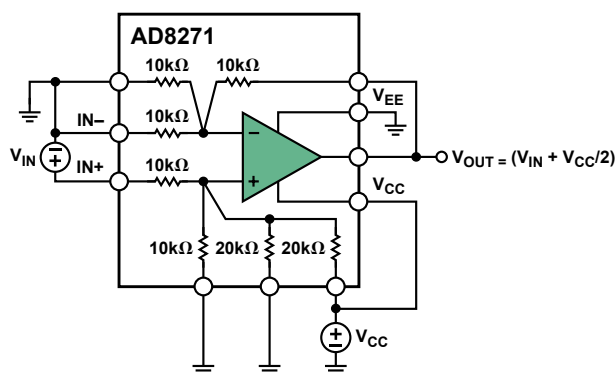


Figure 2. AD8271 shifts output to midsupply with no external components.

Authors

Moshe Gerstenhaber [moshe.gerstenhaber@analog.com] is a Division Fellow at Analog Devices. He began his career at ADI in 1978 and has held various senior positions over the years in manufacturing, product engineering, and product design. Moshe is currently the design manager of the Integrated Amplifier Products Group. He has made significant contributions in the field of amplifier design, especially very-high-precision specialty amplifiers such as instrumentation and difference amplifiers.



Michael O'Sullivan [michael-a.osullivan@analog.com] has worked at Analog Devices since 2004. Currently the product and test engineering manager of the Integrated Amplifier Products Group, he supports product characterization and release of very-high-precision specialty amplifiers such as instrumentation and difference amplifiers. Mike worked as a product engineer in the semiconductor field for over 14 years.



**Analog Devices, Inc.
Worldwide Headquarters**

Analog Devices, Inc.
Three Technology Way
P.O. Box 9106
Norwood, MA 02062-9106
U.S.A.
Tel: 781.329.4700
(800.262.5643,
U.S.A. only)
Fax: 781.461.3113

**Analog Devices, Inc.
Europe Headquarters**

Analog Devices, Inc.
Wilhelm-Wagenfeld-Str. 6
80807 Munich
Germany
Tel: 49.89.76903.0
Fax: 49.89.76903.157

**Analog Devices, Inc.
Japan Headquarters**

Analog Devices, KK
New Pier Takeshiba
South Tower Building
1-16-1 Kaigan, Minato-ku,
Tokyo, 105-6891
Japan
Tel: 813.5402.8200
Fax: 813.5402.1064

**Analog Devices, Inc.
Southeast Asia
Headquarters**

Analog Devices
22/F One Corporate Avenue
222 Hu Bin Road
Shanghai, 200021
China
Tel: 86.21.2320.8000
Fax: 86.21.2320.8222